



Sensitivity of marine heatwaves metrics to SST products, focusing on

the Tropical Pacific

- Carla Chevillard¹, Romain Le Gendre^{2,3}, Christophe Menkes⁴, Takeshi Izumo⁵, Bastien Pagli⁵, Simon
- 4 Van Wynsberge¹ and Sophie Cravatte³
- ¹ Ifremer, UMR 241 SECOPOL (Ifremer, IRD, ILM, UPF), Vairao, Tahiti, French Polynesia
- 6 ² Ifremer, UMR 9220 ENTROPIE (Institut de Recherche pour le Développement, Université de la Réunion, Ifremer, CNRS,
- 7 Université de la Nouvelle-Calédonie), Nouméa, New Caledonia.
- 8 ³ Université de Toulouse, LEGOS (IRD, CNES, CNRS, UT3), Toulouse, France.
- ⁴ IRD, UMR 9220 ENTROPIE (Institut de Recherche pour le Développement, Ifremer, Université de la Réunion, Université
- de la Nouvelle-Calédonie), Nouméa, New Caledonia
- 11 ⁵ IRD, UMR 241 SECOPOL (Ifremer, IRD, ILM, UPF), Faa'a, Tahiti, French Polynesia
- 12 Correspondence to: Carla Chevillard (carla.chevillard@ifremer.fr)

13 Abstract. Marine heatwaves (MHWs) are increasingly studied in climate sciences for their ecological impacts, for which 14 accurate real-time bulletins and forecasts are essential. Yet, methodological choices in their detection affect metric estimates, 15 underlining the need to better assess these sensitivities. This study provides a thorough assessment of the impact of Sea Surface 16 Temperature (SST) product choice on MHW statistics, focusing on the tropical Pacific. MHW detection was performed on six daily gridded SST datasets: four widely used blended satellite observational products, one ocean reanalysis, and a multi-dataset 17 18 ensemble mean computed from the four observational products. Sensitivity to SST products was evaluated for six MHW 19 metrics (MHW days per year, number of events per year, duration, maximum intensity, cumulative intensity and onset rate) 20 and for the Degree Heating Weeks (DHW), a widely used proxy for coral bleaching. Inter-product comparisons revealed a 21 significant dispersion among MHW metric estimates, with the reanalysis GLORYS12v1 detecting fewer, longer and less 22 intense MHWs while OISST detected more MHWs of shorter duration and higher intensity, likely related to their weak and 23 strong high-frequency SST variability (periods shorter than 2 weeks) respectively. The sensitivity analysis showed that the 24 onset rate was the most sensitive metric to SST product choice and the maximum intensity the most robust. Metrics 25 uncertainties were quantified inside seven regions of the basin and were largest in the western Pacific Warm Pool. Co-26 occurrence analyses of MHWs revealed that, over the basin, 10 to 80% of MHW days were detected simultaneously by all 27 products, with the western Pacific Warm Pool showing the lowest agreement (10–40%). Filtering MHWs by size also revealed 28 that the detection of large-scale MHWs ($> 5^{\circ} x 5^{\circ}$) was more consistent across products than smaller ones. Finally, over the 29 studied period, inter-product differences tend to decrease with time. The DHW also revealed to be sensitive to SST products, 30 with inter-product differences on DHW annual maximum reaching more than 1°C.weeks⁻¹ and percentages of bleaching alert 31 days (DHW≥4°C.weeks⁻¹) in common across products reaching 70% at most across much of the basin. These findings 32 contribute to a better understanding of how methodological choices affect the characterization of MHWs and DHW, and their 33 associated uncertainties.



34

3536

37

38

39

40

41

42

43 44

45

46

47

48

49

50

51

52

53

54

55

56

57

58

59

60

61

62

63 64

65 66



1- Introduction

Between April 2023 and July 2024, global ocean surface temperatures reached their highest level ever registered (Terhaar et al., 2025). These extremes observed in global mean Sea Surface Temperatures (SST), partly related to an El Niño event, would not have been reached without the acceleration of ocean warming over the last decades (Merchant et al., 2025). They manifest locally as "marine heatwaves" (MHWs), a term first introduced by Pearce et al. (2011). Hobday et al. (2016) further formalized the definition of a MHW as an episode of temperatures above a climatological threshold for at least five consecutive days, characterized by its duration, intensity, rate of evolution and spatial extent. Due to their significant ecological and biological impacts (Capotondi et al., 2024), MHWs have become a hot topic in ocean science, more so as climate models predict significant increases in their frequency, intensity and duration due to global warming (Frölicher et al., 2018; Oliver et al., 2019). Real-time MHW information and forecasts are of crucial interest to managers and stakeholders as they support marine conservation and fisheries management (Holbrook et al., 2020; Hartog et al., 2023; Hobday et al., 2023; Kajtar et al., 2024; Spillman et al., 2025). Such bulletins must provide accurate information, ideally combined with uncertainty estimates. Explicitly accounting for the methodological choices in MHW detection (Farchadi et al., 2025), and, consequently, quantifying the associated uncertainties, are key to MHW research and to assess their socio-ecological impacts. MHW detection implies several methodological choices: the choice of the SST product, the length of the climatological baseline, whether or not to detrend the SST time series, and the definition of the MHW threshold (Farchadi et al., 2025). If the scientific community agrees on the general methodology - use of 30-year climatology, no detrending and seasonally varying 90th percentile, Hobday et al., 2016 - different options can lead to significantly different results in MHW metrics evaluation potentially leading to different policy responses to MHWs (Capotondi et al., 2024). While the effects of the choice of the climatological baseline (Amaya et al., 2023), of detrending (Smith et al., 2025) and of the use of a fixed threshold (Langlais et al., 2017) have been investigated and discussed, the impact of SST product choice on MHW detection statistics remains little explored. If this step appears crucial for MHW analysis (Farchadi et al., 2025), most MHW studies rely on a single blended SST product, either satellite-only or satellite combined with in situ data, or an ocean reanalysis. A similar issue applies to the Degree Heating Weeks (DHW) computation, a widely-used metric for coral bleaching risk that represents accumulated heat stress which can lead to coral bleaching and mortality (Skirving et al., 2020). This metric is also computed from a single SST product in most coral studies. Yet, SST products differ in their data sources, processing and interpolation methods, and they consequently show variability between themselves (Martin et al., 2012; Dash et al., 2012; Okuro et al., 2014). Several studies have focused on intercomparing satellite-derived SST products, particularly with regard to trends (Menemenlis et al., 2025) or through validations using in-situ observations (Fiedler et al., 2019). Nevertheless, while some studies have shown that MHW characteristics can be biased depending on the chosen SST product (Wang et al., 2024; Lal et al., 2025), the

sensitivity of MHW metrics to the choice of SST product has been scarcely investigated, and to our knowledge, has never been





quantified at global or regional scales. Marin et al. (2021) identified locations where significant differences between products occur, but for coastal MHWs. For DHW, several studies showed significant differences between datasets in specific areas (Neo et al. 2023 compared four datasets in the north western and south western Australian reefs; Margaritis et al. 2025 compared two datasets in the Caribbean).

Such quantification would help to improve the consistency of MHW information and forecasts, which is crucial in basins like the tropical Pacific where communities heavily rely on marine resources (Holbrook et al., 2022; Lal et al., 2025). In this large zone (almost half of the tropics), MHWs are modulated by El Niño Southern Oscillation (ENSO) (Holbrook et al., 2019; Sen Gupta et al., 2020; Pagli et al., 2025), although other phenomena, such as the Madden Julian Oscillation (MJO) (Madden and Julian 1971,1972) and tropical cyclones, can also influence MHW life cycle (Dutheil et al., 2024). There, societies and environments are particularly vulnerable to MHWs (Andréfouët et al., 2015; Smith et al., 2021, 2024), making the tropical Pacific an area of strong interest to MHW research.

The present study consequently provides a quantitative assessment of the sensitivity of MHW metrics to the choice of the SST product, focusing on the tropical Pacific. Six SST datasets are compared: four blended satellite observational products, one reanalysis product, and an ensemble-mean product computed as the average of the four SST observational products. Six MHW metrics (number of MHW days per year, number of events per year, duration, maximum intensity, cumulative intensity and onset rate) are analyzed to determine which metrics are more robust to SST product choice. In addition, the sensitivity to SST products is assessed for the DHW index. A regional approach is also conducted by dividing the tropical Pacific into seven regions and providing spatially averaged uncertainties for MHW metrics and DHW inside these regions, in line with the recommendations of Farchadi et al. (2025) who highlight the importance of accounting for regional variability in MHW studies. The present study is organized as follows. Section 2 describes the data and methodology. Section 3 first provides a comparison of MHW metrics across SST products revealing the impact of high frequency SST variability on MHW detection. A quantitative assessment of the uncertainty associated with the SST product choice is then conducted for each metric at both basin and regional scales, highlighting the highest sensitivity in the western Pacific Warm Pool. Lastly, similar analysis and evaluation of DHW uncertainties linked to the SST choices is also performed. Finally, the results are discussed in section 4.

2- Data and methodology

2.1- SST products

Six SST datasets were used in the study: four observation-based products, their ensemble-mean, and one reanalysis. We used four daily global L4 (Level 4, gap-free, gridded) SST analysis products: the NOAA Advanced very High Resolution Radiometer (AVHRR) Optimum Interpolation (OI) ¼ degree daily SST v2.0 Analysis data (hereafter designed as OISST), the ESA C3S global Sea Surface and Sea Ice Temperature Reprocessed product (hereafter designed as C3S), the global ocean OSTIA SST and Sea Ice reprocessed product, and the NOAA Coral Reef Watch (CRW) version 3.1 daily global 5km SST product known as CoralTemp. These products are among the most commonly used in MHW studies. We also used the ocean





reanalysis GLORYS12v1 as: 1) reanalyses are widely used in MHW research to better understand MHW vertical extent and driving mechanisms (Capotondi et al., 2024; Dutheil et al., 2024), 2) this reanalysis is also used for MHW reports/forecasts by Mercator-Ocean for Copernicus Marine Service¹. The GLORYS12v1 reanalysis used here is a 1/12° reanalysis using the NEMO (Nucleus for European Modelling of the Ocean, Madec et al., 2024) ocean model, forced by ECMWF ERA-Interim atmospheric reanalysis (Dee et al, 2011), complemented by ERA5 re-analyses (Hersbach et al., 2020) for recent years (from January 1st 2019). This reanalysis assimilates sea level anomalies (SLA), observed SST (OISST), sea ice concentration and in situ temperature and salinity vertical profiles (Lellouche et al., 2021).

For MHW inter-comparison, C3S, OSTIA, CRW and GLORYS12v1 were regridded on the OISST 0.25° grid using the conservative method "remapcon" from CDO software (Schulzweida et al., 2023). Finally, a sixth dataset hereafter referred to as "COMPOSITE", was constructed to evaluate the relevance of a multi-product approach for MHW analysis. More precisely, the daily 0.25° COMPOSITE was computed as the mean of the four SST observation-based products: the three re-gridded C3S, CRW and OSTIA, and the raw OISST. The reanalysis GLORYS12v1 was not included in the COMPOSITE since it differs by definition from observation-based products. MHW detection was thus performed on these six 0.25° daily datasets.

Table 1: Description of the SST datasets.

A summary of information for these datasets is provided in Table 1.

Product Reference	Time coverage and temporal resolution	Spatial resolution	Depth	Description and data sources
E.U. Copernicus Marine Service Information (CMEMS). Marine Data Store (MDS) doi:10.48670/moi- 00169	31/08/1981-30/12/2024 Daily	0.05°x0.05°	Representative of the 20cm depth.	Reprocessed SST analysis using temperature from satellites: L3U (A)ATSR, SLSTR, AVHRR, AMSR-E, AMSR-2 v3.0 of ESA SST_cci CRD and ICDR and EOCIS. It is independent from in-situ data.
Coral Temp NOAA Coral Reef Watch (CRW) Skirving et al., 2020	01/01/1985-present Daily	0.05°x0.05°	Representative of the 20cm depth.	Reprocessed SST analysis derived using a combination of 3 L4 nighttime-only satellite SST datasets (two NOAA Geo Polar SST products - Near Real Time and reprocessed - and the 1985-2002 daily global nighttime only foundation SST from OSTIA).
OSTIA E.U CMEMS. MDS doi:10.48670/moi- 00168	30/09/1981 - 31/05/2022 Daily	0.05°x0.05°	SST foundation i.e. SST free of diurnal variability. This is very similar to the temperature measured nominally at a depth of 0.2-1m just before sunrise (Donlon et al., 2012)	Reprocessed SST analysis using satellite data (re-processed ESA SST CCI, C3S [RD.2] EUMETSAT and REMSS) and insitu data from the HadIOD dataset (ships and buoys).

¹ https://www.mercator-ocean.eu/ocean-intelligence/ocean-bulletins-and-insights/marine-heatwaves-archive/

https://doi.org/10.5194/egusphere-2025-5417 Preprint. Discussion started: 13 November 2025







OISSTv2 NOAA Reynolds et al., 2007 Huang et al., 2021	01/09/1981 - present Daily	0.25°x0.25°	Representative of the 20cm depth.	Reprocessed SST analysis using satellite data (AMSR, AVHRR and AVHRR-Only) and in-situ data from ships, buoys and Argo floats.
GLORYS12v1 E.U CMEMS, MDS doi:10.48670/moi- 00021	31/12/1992 - 26/05/2025 Daily	0.08x0.08°	0.49m (minimum depth of the 50 vertical levels)	Ocean reanalysis. Assimilated temperature observations: OISST (Reynolds 0.25° AVHRR-only SST), in situ temperature profiles from Copernicus Marine CORAv4.1 database.
COMPOSITE	01/01/1993-31/12/2021	0.25°x0.25°	-	Mean of the four SST analysis products: C3S, CRW and OSTIA all three re-gridded at 0.25°, and OISST.

2.2- MHW and DHW analyses

2.2.1- Study area

MHW and DHW analyses were performed over the tropical Pacific (30°S - 25°N; 125°E - 70°W, Fig. 1A) at 0.25° spatial resolution. The latitudinal coverage is not symmetric, extending further south to include islands of the southern subtropical Pacific, notably French Polynesia (30°S - 0°S; 165°W - 130°W). As MHW characteristics and ocean processes vary within this area (Holbrook et al., 2019, 2022; Lal et al., 2025), the sensitivity analysis was detailed at regional scale for both MHW metrics and DHW. Seven regions were defined based on the Longhurst et al. (2007) provinces which reflect the ocean's physical and biogeochemical properties. As will be shown later, these regions also correspond to areas with distinct MHW characteristics, and represent different physical regimes in the tropical Pacific. Results of the basin-scale sensitivity analysis were thus aggregated within these regions. They are illustrated in Fig. 1a and named following Longhurst et al. (2007): the North Pacific Subtropical Gyre West (NPSW), North Pacific Tropical Gyre (NPTG), West Pacific Warm Pool (WARM), North Pacific Equatorial Countercurrent (PNEC), Pacific Equatorial Divergence (PEQD), Archipelagic Deep Basins (ARC) and the South Pacific Subtropical Gyre Province (SPSG) (Fig. 1a). Minor adjustments were made to the original WARM province of Longhurst et al. (2007), with a small extension further east to better capture the coherent dispersion patterns of MHW metrics.





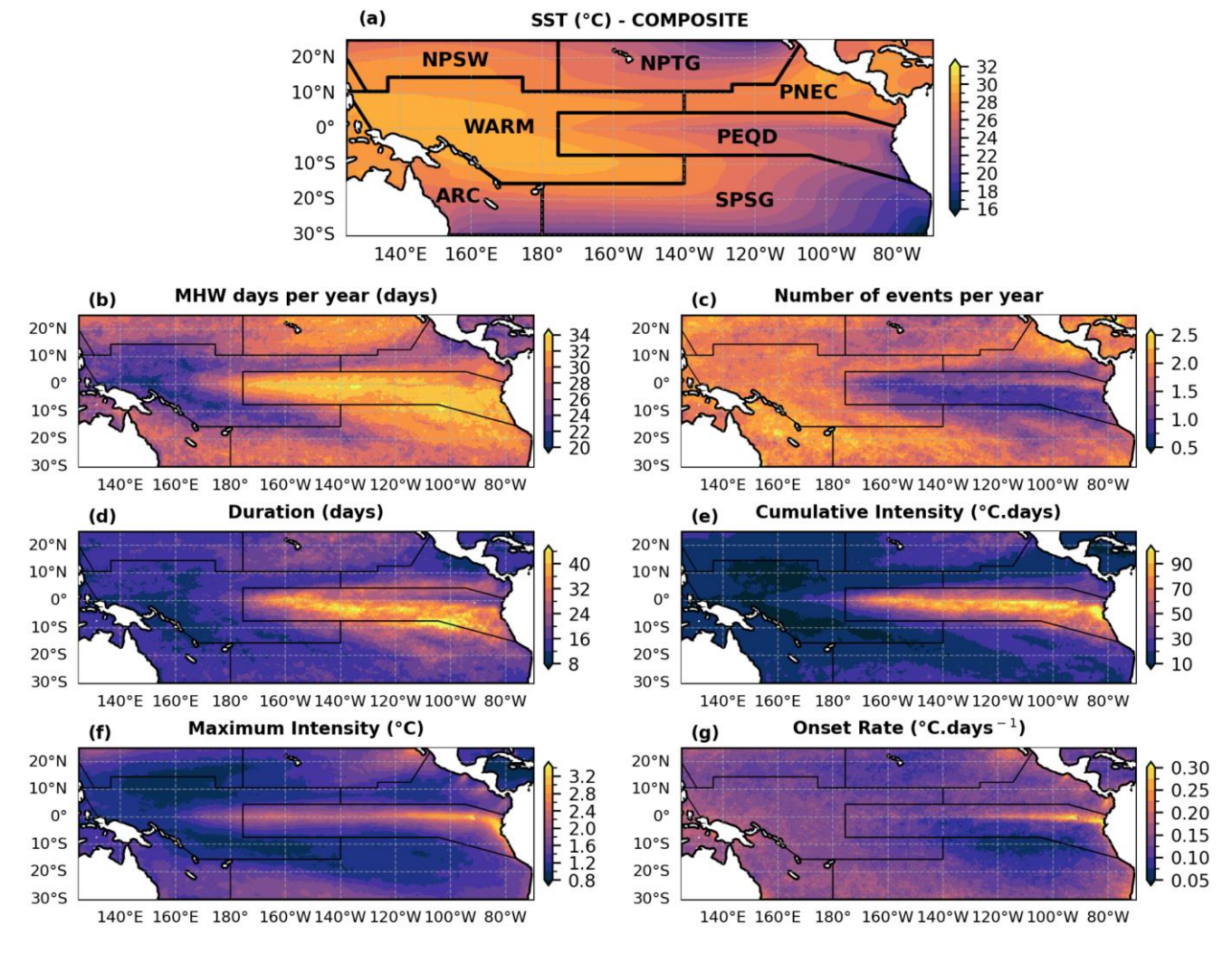


Figure 1: (a) Mean SST (1993-2021) from the COMPOSITE in the tropical Pacific, with the regions of study. (b-g) Ensemble mean of MHW metrics in the tropical Pacific (1993-2021; cf. section 2.3.1), with the limits of the regions defined in (a).

2.2.2- MHW and DHW computation

MHW detection was performed for each pixel of the six datasets presented in section 2.1 on the 0.25° common grid over the tropical Pacific, following the Hobday et al. (2016) method. A MHW event was defined as a period of at least five consecutive days during which SST exceeded the local 90th percentile threshold. Gaps of less than two days within an event were ignored. The analysis was conducted over 1993-2021, which served as the common climatological baseline across the SST products (Table 1, common period to all products). No detrending was applied to the SST time series in order to account for differences in long-term SST trends among products (Menemenlis et al., 2025). The sensitivity analysis was carried out for six MHW metrics: (1) the number of MHW days per year, (2) number of events per year, (3) event duration, (4) maximum intensity, (5)





cumulative intensity, and (6) onset rate. The number of MHW days per year and the number of events per year were defined as the total number of days and events over 1993-2021 divided by the 29 years of the analysis period. Maximum and cumulative intensities were expressed relative to climatology, with cumulative intensity calculated as the sum of daily intensities over each event's duration. The onset rate was defined as the rate of temperature increase from the start of a MHW to its maximum intensity (Hobday et al., 2016).

Daily Degree-Heating Weeks (DHW) values were computed following Skirving et al. (2020) for each pixel of the six SST datasets of section 2.1 at 0.25° resolution. First, daily temperature anomalies (HotSpot) were calculated relative to the local Maximum of Monthly Mean (MMM), defined as the maximum of monthly climatological means over 1993-2021. DHW values on a given day were then computed as the sum over the preceding 12 weeks of daily HotSpot anomalies exceeding 1°C. This accumulated sum was divided by 7 to express DHW in °C weeks -1. Due to its ecological relevance, we investigated the impact of SST product choice on the yearly maximum DHW values in the tropical Pacific. More precisely, this metric quantifies the maximum accumulated heat during a year that can potentially stress marine organisms such as corals.

2.2.3- Filtering MHWs by size

In order to better understand the origin of inter-product differences in MHW metric estimates, MHWs were filtered by size. The sensitivity analysis was carried out for micro (maximum area $\leq 5^{\circ}x5^{\circ}$) and macro (maximum area $\geq 5^{\circ}x5^{\circ}$) events, separately. More precisely, for each day, all pixels where MHWs were detected were assigned a MHW area, defined as the number of contiguous pixels to the studied pixel also experiencing a MHW. These joint pixels were detected thanks to the label function from python package scipy.ndimage (method inspired from Bonino et al., 2023). In a pixel, a MHW was thus associated with a series of areas over its duration. The maximum area reached during the event was associated with each MHW in the evaluated pixel. Events with a maximum area smaller than 25 square degrees were classified as micro-scale, whereas those with a maximum area exceeding 25 square degrees were defined as macro-scale (Lal et al., 2025).

2.3- Sensitivity analysis

2.3.1- Inter-product differences and uncertainty quantification

- Inter-product differences in MHW detection were illustrated by maps of mean MHW metrics for each SST product over the tropical Pacific. For duration, maximum intensity, cumulative intensity and onset rate, these maps were defined at each pixel as the mean value across all MHWs detected between 1993 and 2021. For the number of MHW days per year and the number of events per year, the maps were defined at each pixel as in 2.2.2.
- To better highlight the inter-product differences on MHW metrics, anomalies were also mapped over the tropical Pacific. For each product and metric, the product anomaly at each pixel was defined as the difference between the metric value for that





185

190

197

- product (as defined above) and the ensemble mean value of the metric over the 6 products (i.e. the mean of six values, hereafter
- designated as "ensemble mean" metric) (Eq. 1):
- 173 $anomaly(metric_i, product_j, pixel_k) = metric_i(product_j, pixel_k) ensemble_{mean}(metric_i, pixel_k)$ (1)
- where $ensemble_{mean}(metric_i, pixel_k) = (\sum_{i=1}^{6} metric_i(product_i, pixel_k)) / 6$, with i varying from 1 to 6 and representing the
- six evaluated metrics, j varying from 1 to 6 and representing the 6 evaluated products, and k representing the pixel number in
- the domain. The same maps were produced for the temporal mean of DHW annual maxima (section 2.2.2).
- 178 The sensitivity of each MHW metric to SST product choice was evaluated at each pixel by computing the dispersion of the
- metric across the six SST products (hereafter designated as "ensemble dispersion", Eq. 2).

180
$$\sigma = ensemble_{dispersion}(metric_i, pixel_k) = \sqrt{\frac{1}{6}\sum_{j=1}^{6}[(metric_i(product_j, pixel_k) - ensemble_{mean}(metric_i, pixel_k))^2]}$$
 (2)

- 181 The ensemble dispersion was also computed for DHW. Maps of dispersion over the tropical Pacific were produced for each
- metric. These values of ensemble dispersion were defined as the "uncertainty" of the metric with respect to SST product choice.
- 183 In order to quantify and compare metrics sensitivity, the ensemble dispersion at each pixel was also expressed as a percentage
- by dividing the ensemble dispersion by the ensemble mean value of the metric at that pixel, and then multiplying by 100.
- The co-occurrence of MHWs across SST products was also assessed by computing the percentage of common MHW days
- over the basin. At each pixel, this percentage was defined as the number of days detected simultaneously as a MHW in all six
- products divided by the ensemble mean number of total MHW days at that pixel. Similar analysis was conducted for DHW,
- by computing the percentage of common bleaching alerts of level 1 (days for which DHW\ge 4°C.weeks-1) across products.

2.3.2- Temporal evolution

- 191 The temporal evolution of MHW metrics sensitivity to SST product choice was evaluated by computing yearly time series of
- ensemble dispersion for each metric and region. For this purpose, yearly maps of MHW metrics and ensemble dispersion over
- the tropical Pacific were produced, following the method described in section 2.3.1. The year attribution of a MHW was based
- on its time start. Then, spatial averages of these yearly values of ensemble dispersion were computed within each region, to
- yield one annual dispersion value per metric and region. The spatial average of ensemble dispersion values inside a region was
- yield one annual dispersion value per metric and region. The spatial average of ensemble dispersion values histor a region was
- computed for a given year if dispersion values could be computed for at least 10% of the pixels of the region.
- 198 The temporal evolution of metrics sensitivity to SST product choice was also assessed by computing yearly time series of
- 199 inter-product spatial correlation within all regions (hereafter designated as "ensemble spatial correlation"). For each region
- and year, spatial correlation between pairs of products was quantified using the uncentered statistic of pattern correlation
- methods (Barnett and Schlesinger, 1987), which correlates fields without removing the spatial means. The uncentered statistic
- was used here since IPCC reports argue that it is better suited for detection in pattern correlation studies as it includes the



204

205

206207

208

209

210

211

212

213

214

215

216

217

218

219

220

223

225

226

229

231

232

233



response in the global mean, while the centered statistic is more appropriate for attribution because it better measures the similarity between spatial patterns (IPCC, 2001). The uncentered pattern correlation statistic is defined in Eq. 3:

$$PatternCorrelation (product_a, product_b) = \frac{\sum_{k=1}^{n} a_k b_k}{\sqrt{\sum_{k=1}^{n} a_k^2 \sum_{k=1}^{n} b_k^2}}$$
(3)

where a and b represent yearly metric values for two SST products inside the region evaluated (n pixels in the region).

The value of pattern correlation was considered when the associated p_value (based on t-test) was inferior to 0.01. For a given metric, region and year, the pattern correlation was computed for all 15 product pairs, and these 15 values were averaged to give the yearly value of the ensemble spatial correlation in the region studied. The spatial correlation inside a region was computed for a given year if ensemble spatial correlation values could be computed for at least 10% of the pixels of the region.

3- Results

3.1- MHW characteristics in the Tropical Pacific

Ensemble mean MHW metrics over 1993-2021 are shown in Fig. 1 in the tropical Pacific, with patterns reflecting spatial variability associated with ENSO. In the central and eastern Equatorial Pacific (PEQD), ENSO largely drives MHW risk (Holbrook et al., 2019; Capotondi et al., 2022). Although MHW occurrences are relatively low in this area (Fig. 1c), the number of MHW days per year is highest, exceeding 32-34 days (Fig. 1b). Here, MHWs have longer durations as they last between 30 to more than 50 days on average (Fig. 1d), and exhibit the highest maximum intensity (more than 3.5°C, Fig. 1f) and cumulative intensity (more than 100°C.days, Fig. 1e) (Holbrook et al., 2019; Oliver et al., 2021). The highly intense MHWs observed in a narrow band along the Equator (2°S-2°N) near the South American Coast are also associated with the highest onset rates of the tropical Pacific (more than 0.3°C/days, Fig. 1g).

In the northeastern tropical Pacific (NPTG), MHWs occur on more than 30 days per year (Fig. 1b) but the number of events is low (~ 1 per year, Fig. 1c). These events are relatively long (30 days, Fig. 1d) and intense (cumulative intensity of 40-

50°C.days, Fig. 1e). In contrast, the PNEC experiences one of the highest numbers of events (more than 2.5 per year, Fig. 1c,

224 also observed by Holbrook et al., 2019; Oliver et al., 2021). This area, influenced by the equatorial countercurrent dynamics,

is characterized by short (less than 15 days, Fig. 1d) but intense events, with maximum intensity reaching 2.5°C (Fig. 1f).

These features are likely linked to the high SST variability of the region, which favors strong MHW intensities (Oliver et al.,

227 2021).

In the southwest tropical Pacific (mainly ARC), MHW occurrence is modulated by La Niña conditions (Sen Gupta et al., 2020;

Lal et al., 2025). Mesoscale eddies close to the eastern Australian coast (Bian et al., 2023; Chapman et al., 2025) along with

downwelling Rossby waves and downwelling-favourable winds also favor MHW development (Misra et al., 2021; Li et al.,

2023). In this region, MHWs are relatively frequent (more than 2 events per year, Fig. 1c) but short (less than 15 days Fig. 1d,

Holbrook et al., 2019). Both the number of MHW days and the maximum intensities are close to the tropical Pacific average

(around 25 days and 1.5°C, respectively, Fig. 1b,f). Similar MHW characteristics are observed in the western SPSG and in



239

240

241

242

243

244

245

246

247

248

249

250

251

252

253

254

255

256

257



NPSW. The northeastern part of the SPSG close to the PEQD is rather influenced by ENSO, with fewer MHWs of longer duration and lower onset rate. The shortest MHWs (less than 10 days, Fig. 1d) are observed in the WARM region. Here, the number of MHW days per year, as well as the cumulative and maximum intensities reach their lowest levels in the tropical Pacific (~15 days per year, <10°C.days and 1°C, respectively). Nevertheless, this region records a high number of events with more than 2.5 events per year close to the Indonesian coast (Fig. 1c, also observed in Holbrook et al., 2019; Oliver et al., 2021).

The MHW analysis performed over the six SST datasets reveals significant differences across products, as illustrated by the

3.2- Inter-product comparison and ranking

MHW days per year computed for each product (Fig. 2a-f). The associated maps of anomalies (Fig. 2g-l; section 2.3.1) allow us to more easily identify potential outliers. Figures S1-S5 extend the inter-product comparison to the other metrics. If the main spatial patterns of mean MHW metrics described in section 3.1 are common between all products, Fig. 2 and Fig. S1-S5 highlight that values can differ by almost a factor of two between products. For the MHW days per year (Fig. 2a-f), the largest differences are observed in the WARM region, with GLORYS12v1 detecting 30 MHW days per year while OISST detects around 15 days per year. Anomalies relative to the ensemble mean range approximately between ±5 days per year inside the tropical Pacific, with some areas showing even larger anomalies (Fig. 2g-l). The strongest positive (negative) anomalies are observed for GLORYS12v1 (OISST). GLORYS12v1 systematically detects more MHW days than the other products, and OISST less MHW days. C3S and OSTIA show smaller anomalies for this metric. For all products, anomalies are closer to zero in the PEQD, a region of strong influence of ENSO where the longest MHWs are observed (section 3.1). For the other metrics, anomalies generally remain within ± 0.5 events per year, ± 10 days for MHW duration, ± 0.25 °C for maximum intensity, ±15°C.days for cumulative intensity and ±0.15°C/days for onset rate over the tropical Pacific (Supplementary Fig S1-S5). As for the MHW days per year, anomalies for the other metrics reveal that GLORYS12v1 and OISST show the largest anomalies, whereas C3S, CRW and OSTIA are closer to the ensemble mean - except near the Indonesian coast where OSTIA shows strong positive anomalies in event frequency and onset rate. Unlike the number of MHW days per year, anomalies for other metrics vary substantially in space, and can be either positive or negative within the tropical Pacific for the same product (especially for the number of events per year).





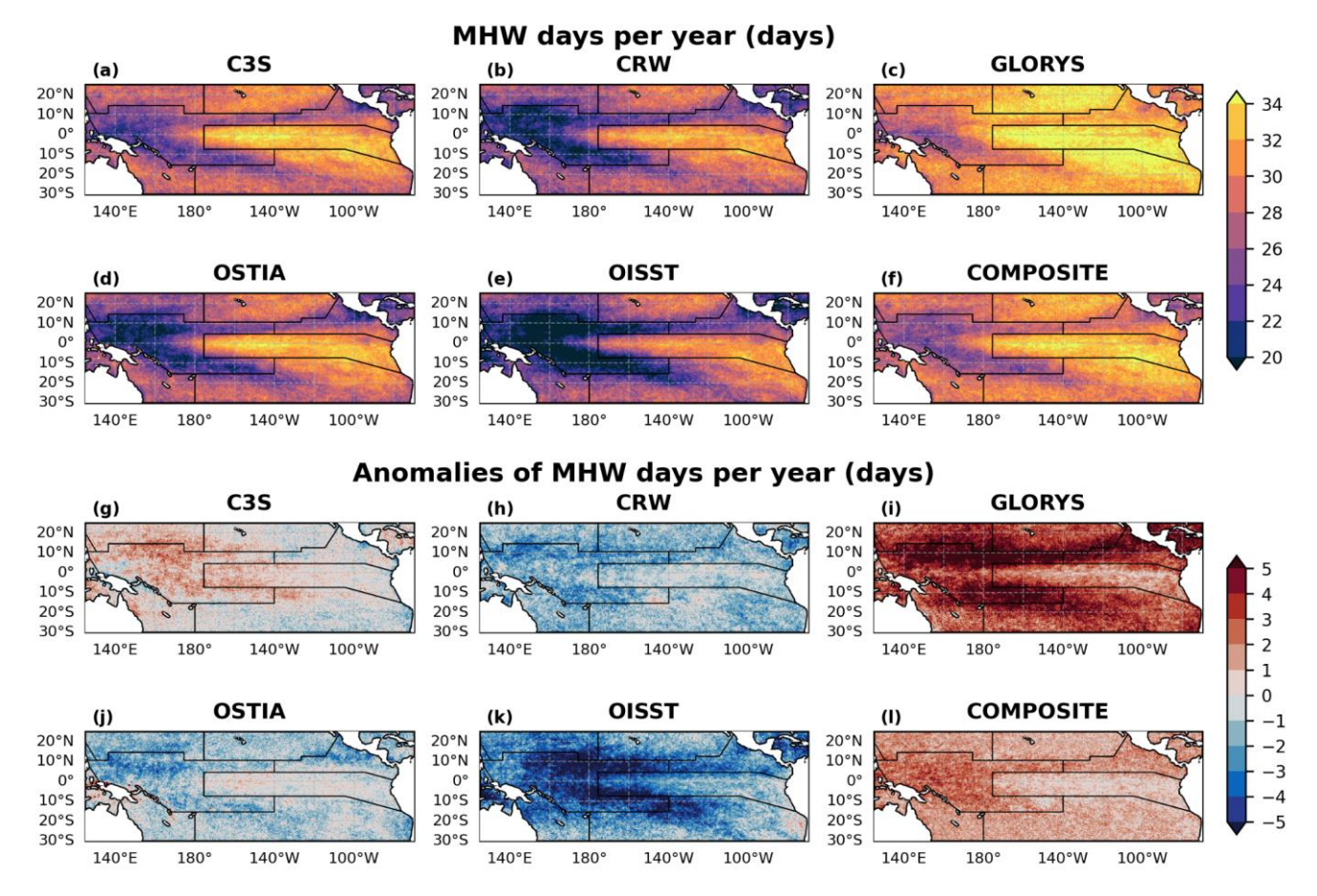


Figure 2: (a-f) Number of MHW days per year over the period 1993-2021 for the six SST products. (g-l) Anomalies of MHW days per year for each product relative to the ensemble mean (section 2.3.1). Black lines indicate regions' limits.

To summarize inter-product differences, the average of MHW metrics for all events detected in the tropical Pacific during 1993-2021 were computed for each product (Fig. 3). In the study area, OISST ranks first for maximum intensity, onset rate, and the number of events detected. By "ranking", we only mean to compare products but not to determine if one performs better than another. Conversely, OISST shows the lowest ranking for the number of MHW days, duration and cumulative intensity (Fig. 3). The opposite pattern is observed for GLORYS12v1 reanalysis which shows the highest ranking for duration, cumulative intensity and the number of MHW days detected, while it ranks last for MHW maximum intensity and onset rate. The COMPOSITE product tends to follow the rankings of GLORYS12v1, with radar charts showing similar shapes (Fig. 3). OISST and GLORYS12v1 therefore stand out in this study, consistently occupying either the lowest or highest ranks across MHW metric estimates. By contrast, C3S shows a more "balanced" radar chart, with no clear overestimation or underestimation compared to other products. These findings are consistent with the anomaly analysis presented in Fig. 2 and Fig. S1-S5.





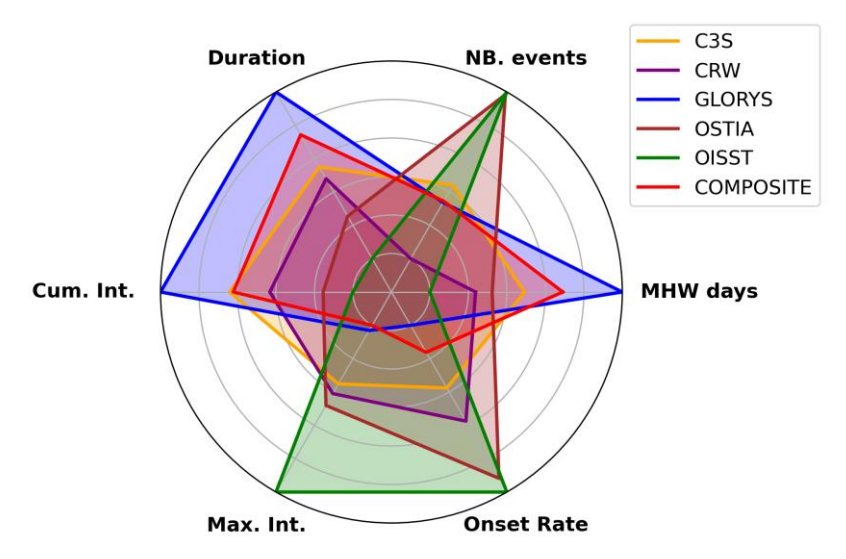


Figure 3: The radar chart is a comparison of all product metrics. The average of MHW metrics are computed for all events detected in the tropical Pacific over 1993-2021 for each product, and normalized by the product that reaches the maximum metric so that all values of the radar chart vary between 0 and 1 (plotted along the radial axes).

The comparison of MHW metrics between products thus highlighted significant differences which vary spatially and between metrics. In the next section, the robustness of the different metrics regarding SST choices is evaluated by quantifying the uncertainty linked to the SST product choice for each metric at both tropical Pacific and regional scales.

3.3- Uncertainty in MHW metrics due to the SST product choice

3.3.1- Basin-scale overview and regional quantification

The MHW co-occurrence analysis (section 2.3.1) reveals that over the basin, between 10 and 80% of MHW days are detected simultaneously by all six products (Fig. 4a). Excluding the PEQD region, where percentages reach their maximum ranging between 60 and 80%, MHW days in common do not exceed 50% over the tropical Pacific and even drop below 20% in a large part of the basin, in the WARM and PNEC regions. The spatial patterns of common MHW days match well with precipitation contours in the basin (Fig. 4a), an aspect further discussed in section 4.2.

The ensemble dispersion normalized by the ensemble mean for each MHW metric (Fig. 4b-g, section 2.3.1) highlights that the onset rate is the most sensitive metric to inter-product variability. Dispersion for this metric exceeds 30% across much of the tropical Pacific, reaching values above 50% in the southeastern part of the basin (around 10°S-130W, Fig. 4g), where onset rates are small (Fig. 1g). MHW duration also exhibits high sensitivity to the choice of SST product, with normalized dispersion ranging between 20 and 30% over the basin, closely followed by the cumulative intensity and the number of events per year (Fig. 4c,d,e). The MHW days per year and the maximum intensity show the lowest dispersion, with values ranging between 0-5% (in the PEQD) and 20% (30%) for the maximum intensity (total MHW days) (Fig. 4b,f).

The high ensemble dispersion values observed in the WARM region across all metrics (Fig. 4b-g) is consistent with the small fraction of MHW days detected simultaneously by all six products in this area (between 10 and 20%, Fig. 4a). The spatial patterns of common MHW days also show good correspondence with dispersion patterns of the total MHW days per year and maximum intensity (Fig. 4b,f), with high dispersion coinciding with a low percentage of common days, and vice versa.

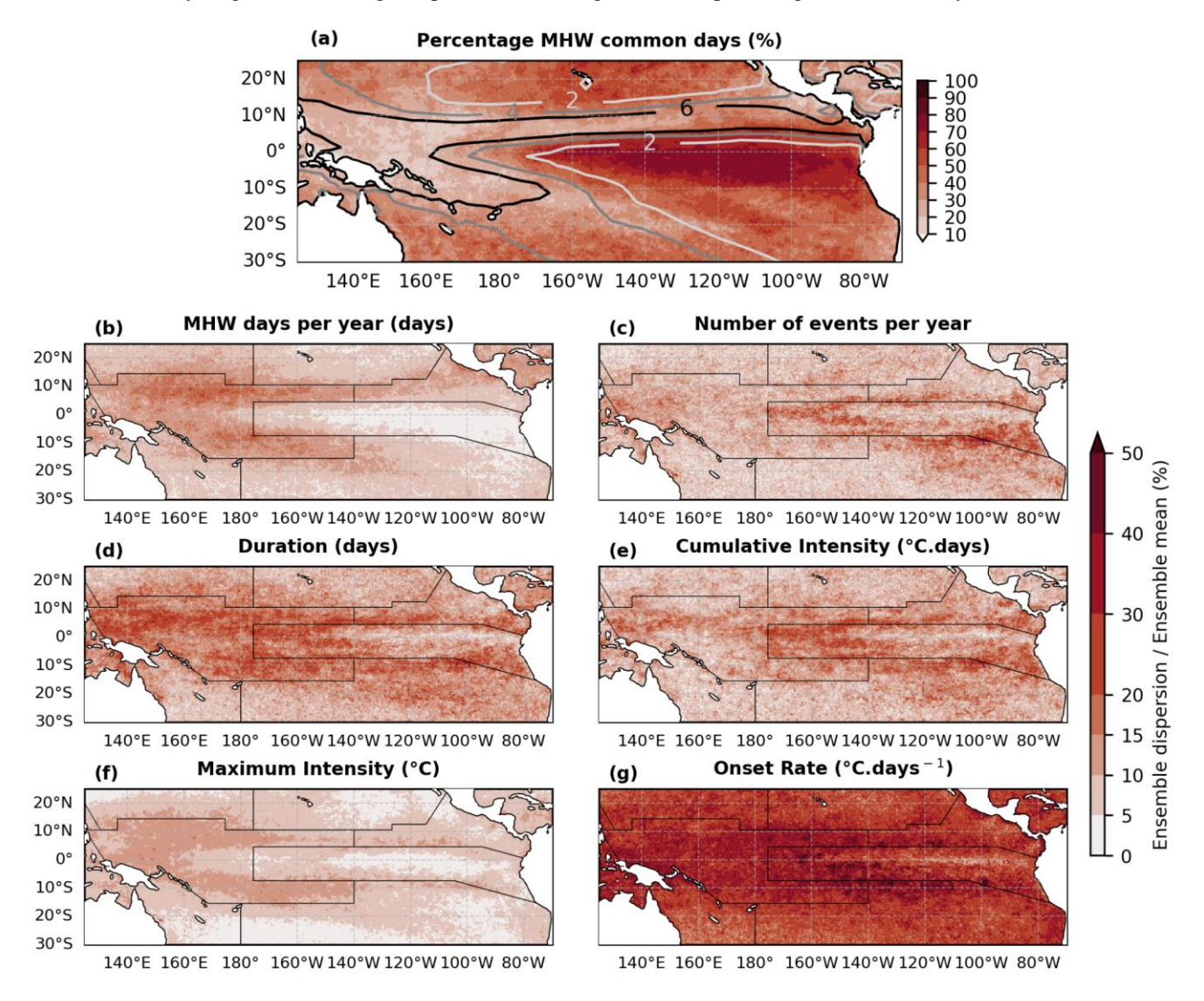


Figure 4: (a) Percentage of MHW days detected simultaneously by the six SST products (section 2.3.1), with ERA5 precipitation contours overlaid (temporal average over 1993-2021, in mm/day). (b-g) Normalized ensemble dispersion for each MHW metric (value in %, section 2.3.1). Black lines indicate regions' limits.

The spatial variability of the previous results supports the need of a regional approach in our sensitivity analysis. Consequently, spatial boxplots of dispersion values within each region are represented in Fig. 5. Across regions, the dispersion distributions



306

307

308

309

310

311

312

313

314

315

316

317

318

319

320

321

322

323

324



is detailed in Fig. 5 (exact value), providing the uncertainties for each metric and region. The regional analysis (Fig. 5) confirms the basin-scale findings (Fig. 4): the onset rate and duration metrics are the most sensitive metrics to SST product choice, with uncertainties exceeding 10% of the regional means in all regions and peaking in the WARM (33.2% for the onset rate, Fig. 5). Cumulative intensity also shows uncertainties larger than 10% in all regions except NPSW and ARC. The number of events per year exceeds 10% uncertainties in three of the seven regions - WARM, PNEC and PEQD (Fig. 5). Finally, the total MHW days per year and maximum intensity are the least impacted metrics with uncertainty lower than 10% in all regions except WARM (and PNEC for MHW days per year). Fig. 5 also highlights the WARM as the most sensitive region to SST product choice, since percentages of dispersion are higher than 10% whatever the metric. It is closely followed by the PNEC, with uncertainties higher than 10% for all metrics except maximum intensity. Conversely, NPSW and ARC are the regions that exhibit the lowest uncertainties. The PEQD shows some of the lowest dispersion values among all regions for the total MHW days per year and maximum intensity, but for all other metrics dispersion exceeds 10% of the ensemble mean. Moreover, the PEQD shows important dispersion outliers for all metrics which are two to three times larger than in other regions for the duration and cumulative intensity (reaching 20 days and 35°C.days, respectively, a pattern also observed in SPSG probably due to ENSO induced variability). The outliers are important as they provide further insights on metrics uncertainties. For example, in PEQD, MHWs detected have an uncertainty of ±0.11°C in maximum intensity with respect to inter-product differences (average dispersion value, Fig. 5). However, some dispersion values inside this region can reach more than 0.5°C (Fig. 5), suggesting that MHW analyses inside PEQD should

be interpreted with caution if based on a single dataset (almost 1°C of uncertainty for some pixels inside this region).

for each metric differ significantly (Mann–Whitney test, p < 0.05). The spatial average of dispersion values within each region



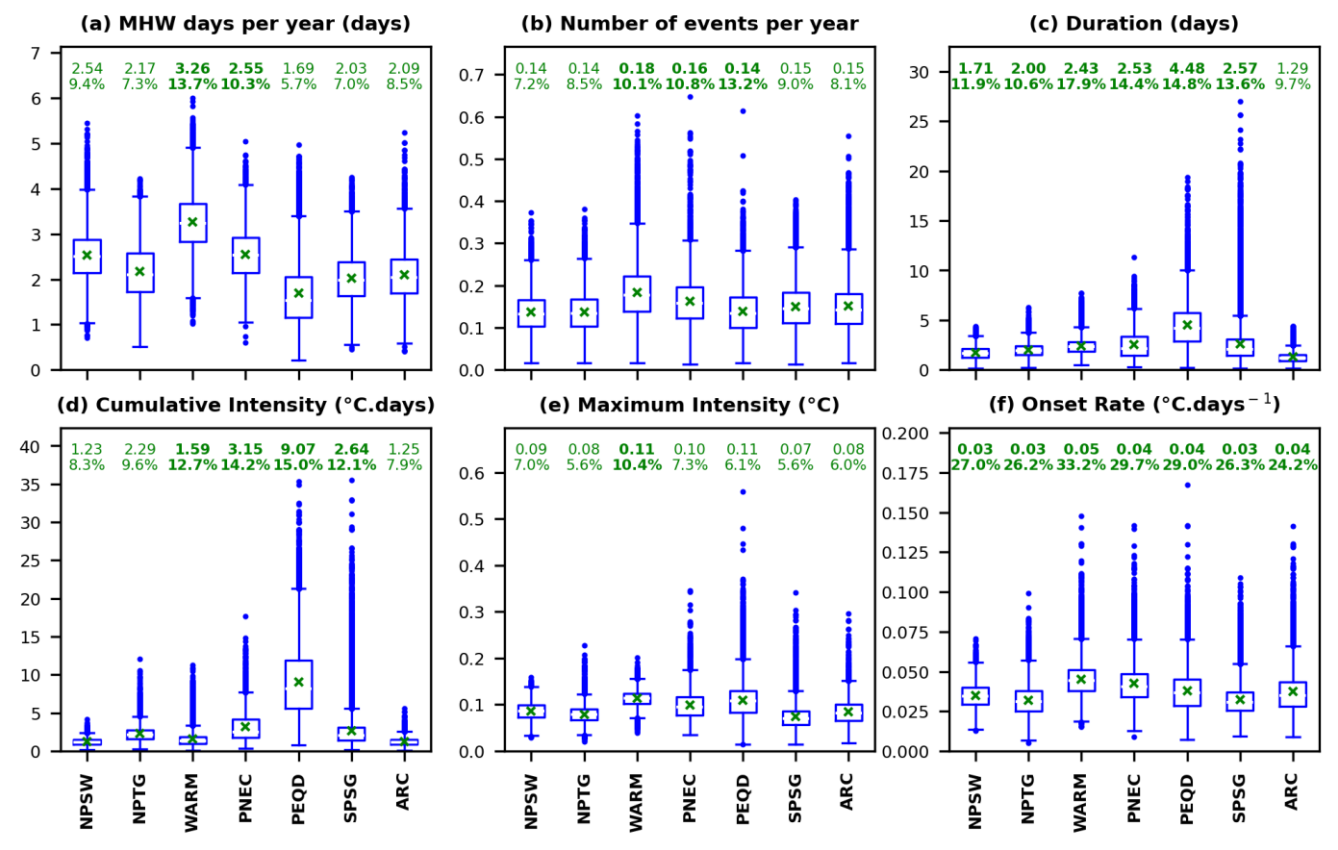


Figure 5: Spatial boxplots of the ensemble dispersion values from Fig. 4b-g for each region. Boxes contain 50% of the values (limits are the first quartile Q1 and third quartile Q3), with the green marker representing the mean value. Whiskers (lines extending from the box) represent the typical range of data; they extend from Q1 - 1.5 \times (Q3-Q1) to Q3 + 1.5 \times (Q3-Q1). The dots outside the whiskers are considered as "outliers". The exact mean value (green marker) is indicated at the top of each boxplot (1st number from the top), along with its equivalence in percentage of the ensemble mean in the region (2nd number from the top). Mean dispersions higher than 10% of the regional mean value are highlighted in bold.

3.3.2- Metrics uncertainty as a function of MHW size

We now examine whether the metrics sensitivity to the SST product depends on the size of the MHWs. We investigated this hypothesis by filtering MHWs by size (section 2.2.3), and ensemble dispersion was then computed separately for macro and micro-scale events. Spatial patterns of macro ($> 5^{\circ}x5^{\circ}$) and micro events (Fig. 6a,b,c,d) show that macro events occur mainly in regions influenced by ENSO (PEQD and southeastern SPSG) while micro events are mainly concentrated near coastlines and at the southern and northern limits of the study area (in the PNEC, WARM, ARC, but also northern NPSW and in SPSG near the shore).

Very few micro-scale MHW days are detected simultaneously by all SST products (Fig. 6f): percentages of MHW common days range between 40% in areas where micro-scale events are numerous and less than 5% where they are fewer. In contrast, percentages of MHW days in common for macro scale events range between 20% in the WARM (where they are fewer) and





80% in the PEQD (Fig. 6e). Differentiating macro and micro-scale events highlights that dispersion is generally lower for macro-scale events (Fig. 6g). This is particularly striking for the total MHW days per year and number of events per year, for which ensemble dispersion decreases by more than two between micro- and macro-scale events (spatial average over the basin). Dispersion for cumulative intensity, maximum intensity and onset rate remains slightly lower for macro-scale events compared to micro-scale events, but is slightly higher for duration.

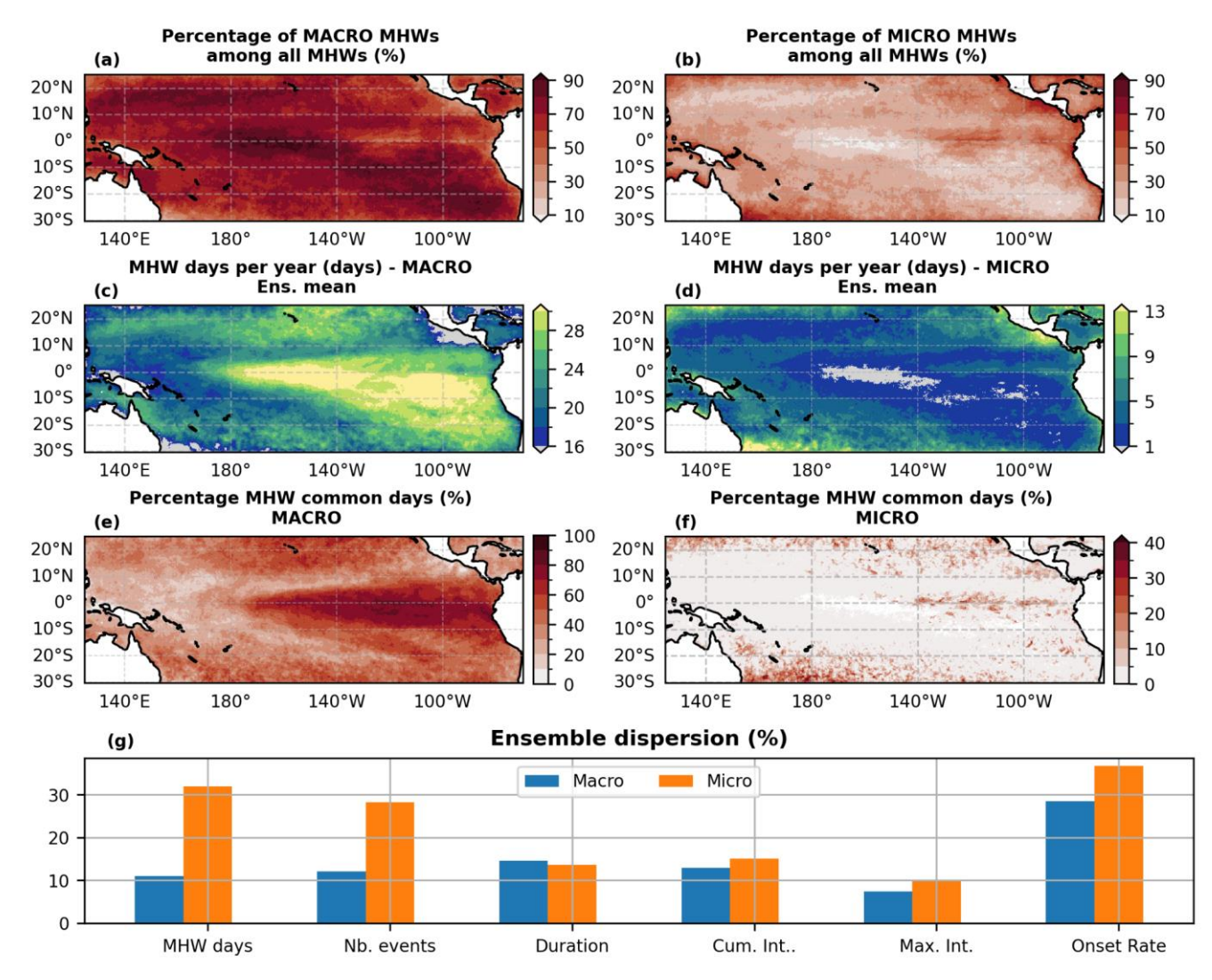


Figure 6: (a) Percentage of macro-scale MHWs among all events detected over 1993-2021 (i.e. ensemble mean of the total number of macro events divided by the ensemble mean of the total number of MHWs of all types, multiplied by 100). (b) Same as (a) for micro-scale MHWs. (c) Ensemble mean of total MHW days per year for macro scale events. (d) Same as (c) for micro-scale MHWs. (e) Percentage of MHW days detected in common by all six products (section 2.3.1) over 1993-2021 for macro scale events. (f) Same as (e) for micro-scale MHWs. (g) Spatial average over the tropical Pacific of dispersion values for each metric for macro-scale MHWs (blue bars) and micro-scale MHWs (orange bars).





3.3.3- Temporal variability of the dispersion

Having quantified inter-product differences, we investigated their temporal evolution to assess both long-term trends and the influence of ENSO events on their temporal variability. The yearly time series of MHW metrics averaged over the tropical Pacific for each product highlight the inter-annual variability of inter-product differences (black line Fig. 7), which appears to vary between metrics. Over the basin, differences between products are rather stable through years for the maximum intensity and onset rate while they seem to increase for years marked by strong El Niño events (1997-98, 2015-16) for the other metrics (Fig. 7). The particularly high values in 2015 compared to 2016 for the metrics duration, cumulative intensity, maximum intensity and rate of onset is explained by the year attribution of MHWs to its time start and the starting of the strong El Niño event in 2015.

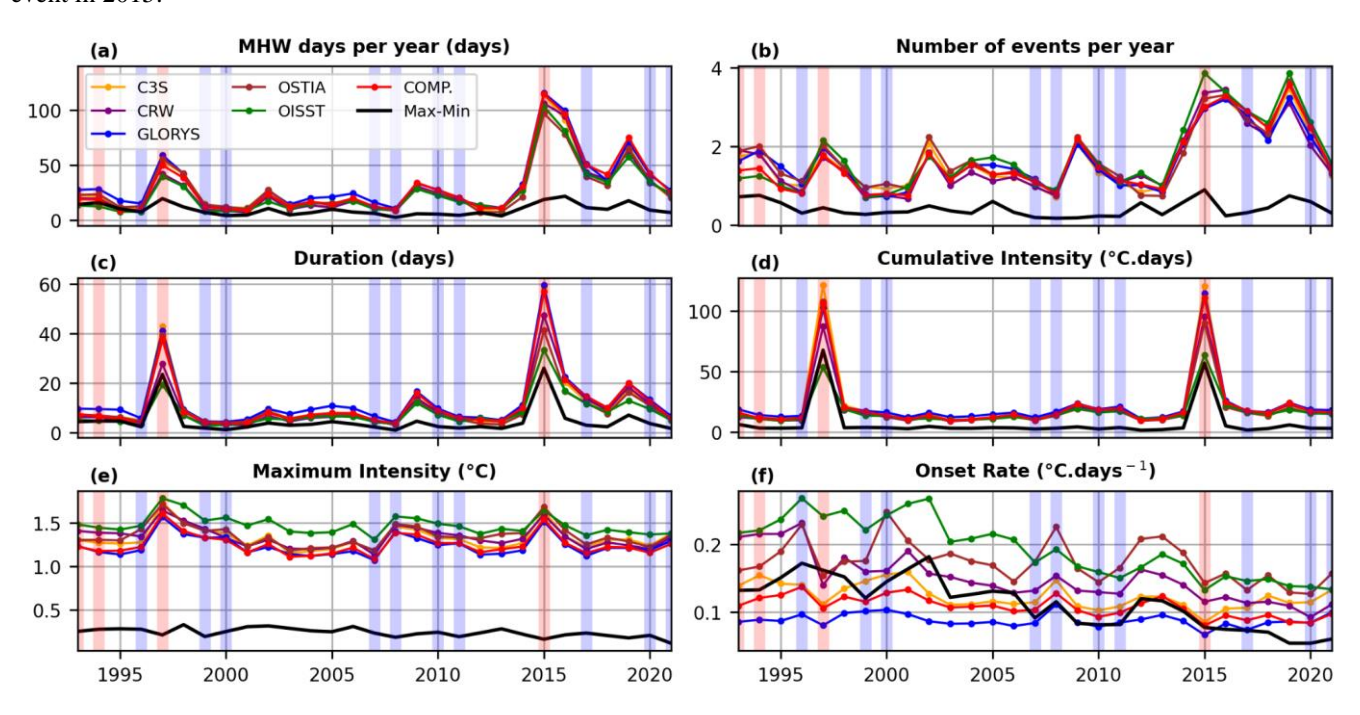


Figure 7: (a-f) Yearly time series of MHW metrics averaged over the tropical Pacific for each product. Inside each panel, the black line represents the largest inter-product difference value for each year (maximum-minimum). The red and blue backgrounds indicate years of strong El Niño and La Niña, respectively, according to the Meiv2 index.

The yearly time series of the ensemble dispersion and spatial correlation within each region (section 2.3.2, Fig. 8 and Fig. S6) provide more insights on the temporal evolution of inter-product differences, and highlight four main points. First, the ensemble dispersion and ensemble spatial correlation values are coherent: metrics showing the lowest dispersion (maximum intensity and MHW days per year) also exhibit the highest ensemble spatial correlation (values ranging between 0.8 and 1), whereas metrics showing the highest dispersion (onset rate) show the lowest ensemble spatial correlation (values ranging between 0.4 and 0.6). The number of events per year, the duration and the cumulative intensity fall in an intermediate range.



374

381

382

384

385

387

388

391

393

394



375 all metrics. 376 Second, yearly ensemble dispersion values are higher than those computed on the mean of metrics as in Fig. 4 since the yearly 377 filter implies more restrictions in MHW comparison. This suggests that ensemble dispersion might be underestimated when 378 computed on the mean of metrics over a long period. 379 Third, the long-term trends suggest a reduction in the inter-product dispersion and an increase in the spatial correlation over 380 the period 1993-2021 for all metrics and regions (Fig. 8 and Fig. S6). In all regions, the largest decreases in ensemble dispersion are observed for the total MHW days per year and the onset rate (-6.6%/dec in WARM and -7.2%/dec in NPSW, respectively, p_values<0.05) while the lowest ones are observed for the maximum intensity (between -1.1%/dec and -2.7%/dec in SPSG 383 and WARM, respectively, p value<0.05). The highest increasing rates of ensemble spatial correlation are also observed for the total MHW days per year and the onset rate, reached in the WARM and NPSW, respectively. Fourth, ensemble dispersion and spatial correlation show an interannual variability partly linked to ENSO variability. For both 386 statistics, MHW days per year shows the highest interannual variability which is marked by the strong El Niño years of 1997-98 and 2015-16 (minima of dispersion and maxima of spatial correlation). On the contrary, the maximum intensity shows the lowest interannual variability among metrics (Fig. 8 and SP7). Yet, the effects of ENSO variability on ensemble dispersion 389 and spatial correlation depend on various factors. They can vary between metrics inside a same region: in the PEQD (where 390 the effects of ENSO are strong), dispersion is lower for strong El Niño years (1997-98, 2015-16) for the total MHW days per year while it is higher for the duration, number of events per year, cumulative intensity and onset rate (Fig. 8a-f). Similar 392 results are observed in the WARM and SPSG. The effects of ENSO variability can also vary between regions for a same metric: duration shows higher spatial correlations for strong El Niño years in most regions but not in WARM and SPSG where

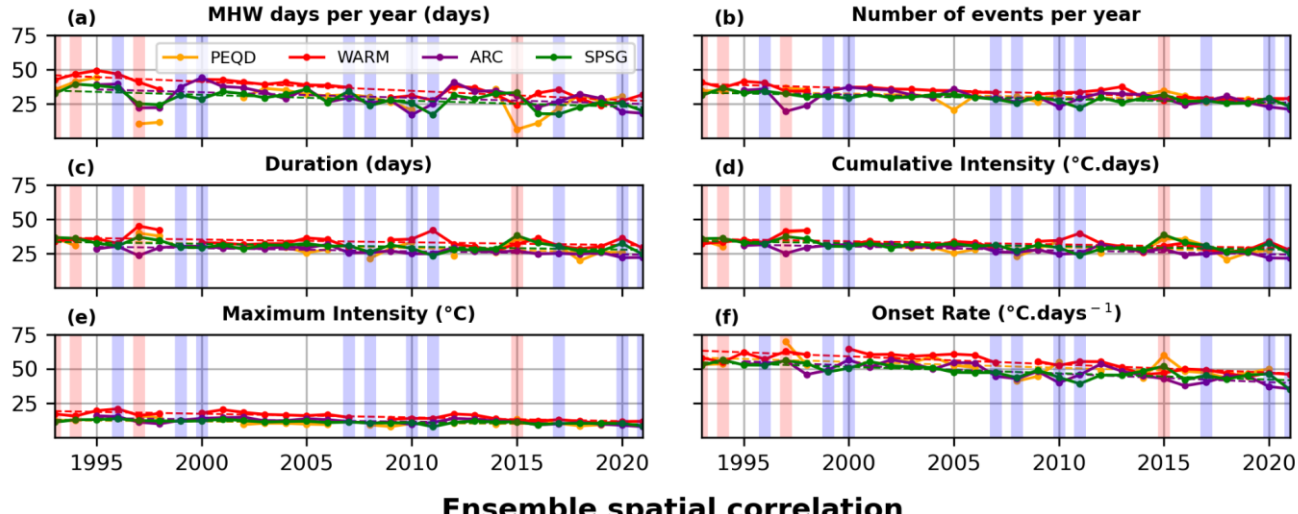
spatial correlation is lower these years and maxima is reached in 2011 (La Nina) in SPSG (Fig. 8i).

The WARM region also shows some of the highest and lowest values of dispersion and spatial correlation, respectively, across









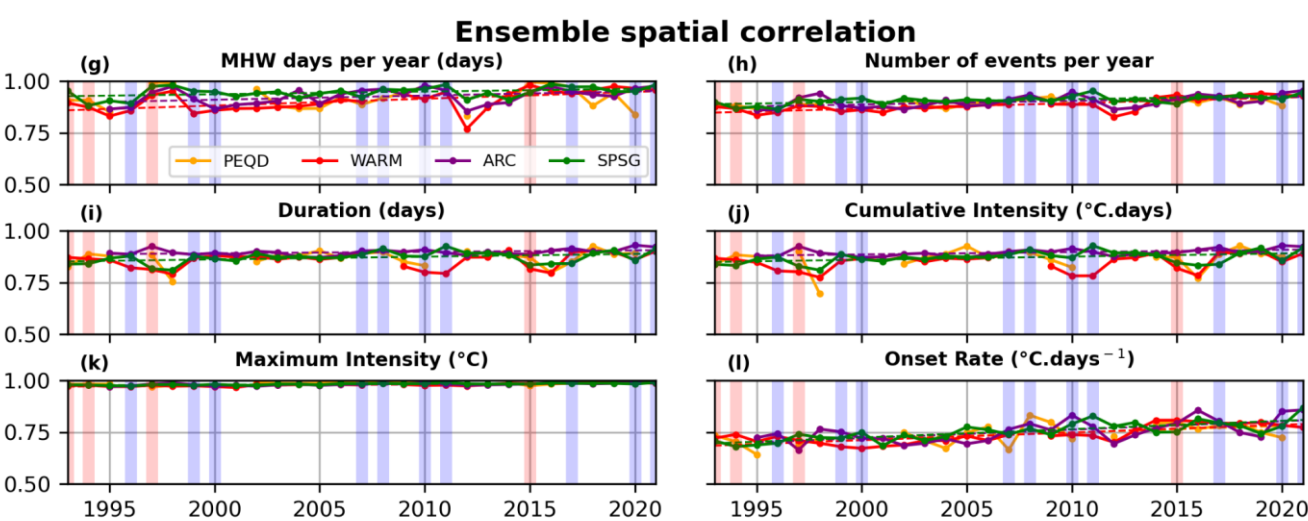


Figure 8: (a-f) Yearly time series of ensemble dispersion (in percentage) for PEQD, WARM, ARC and SPSG. The dashed lines indicate the significant linear trends (p_value<0.05). The red and blue backgrounds indicate years of strong El Niño and La Niña, respectively, according to the Meiv2 index. (g-l) Same as (a-f) for the ensemble spatial correlation (section 2.2.3). Time series in the PNEC, NPTG and NPSW are represented in Supplementary Fig. S6.

Once inter-products differences were quantified for MHW metrics, they were also analysed for the DHW index, a widely used proxy for coral bleaching.

3.4- Uncertainty in the bleaching alerts (Degrees Heating Weeks)

The temporal mean of DHW annual maxima over 1993-2021 in the tropical Pacific (Fig. 9a-f) highlights the influence of ENSO on the DHW, with highest values being observed in the central and eastern Equatorial Pacific (more than 5 °C.weeks⁻¹) for all products. Such influence is also seen on the yearly time series of DHW annual maximum for each product (Fig. 10a,





spatial average over the tropical Pacific), with maxima observed in strong El Niño years of 1997-98 and 2015-16. Figure 9 highlights significant inter-product differences for DHW annual maximum, with anomalies ranging between ±0.5°C.weeks⁻¹ (Fig. 9g-l), and even higher in the western and central eastern equatorial part of the basin. Over the tropical Pacific, the highest positive anomalies are observed for OISST and C3S while the highest negative anomalies are observed for GLORYS12v1. Inter-product differences of more than 1°C.weeks⁻¹ are observed between C3S and GLORYS12v1 in the PEQD close to the south American coast (80°W, 0°) and between OISST and GLORYS12v1 in a large area around (140°E, 10°S), between northern Australia and Indonesia.

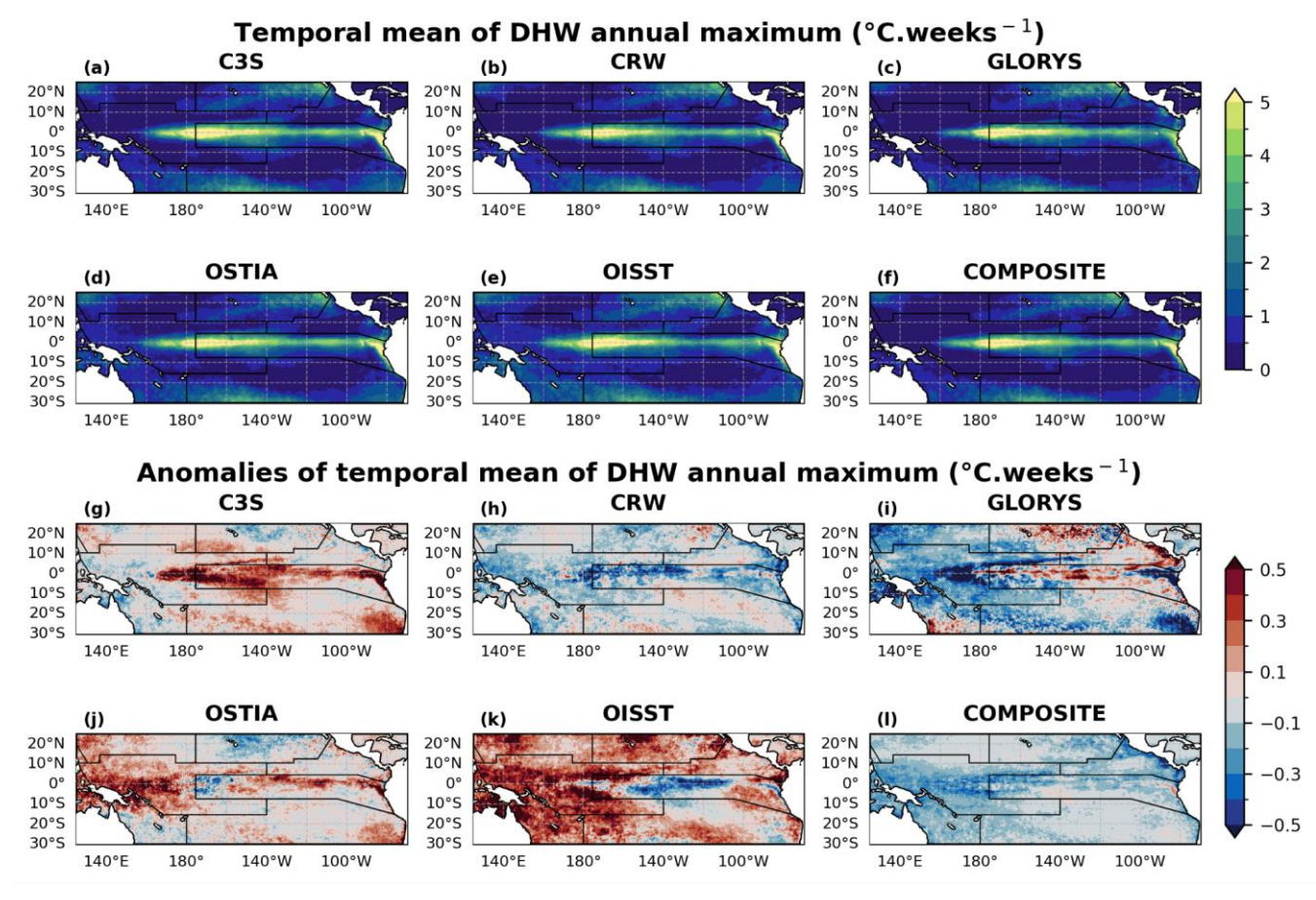


Figure 9: (a-f) Temporal mean of DHW annual maximum over the period 1993-2021 for the six SST products. (g-l) Anomalies of the temporal mean of DHW annual maximum for each product relative to the ensemble mean (section 2.3.1). Black lines indicate regions' limits.

Figure 10a confirms that over the years, OISST detects the highest annual maxima of DHW, except in years of strong El Niño (1997-98, 2015-16) where C3S shows the highest annual DHW maximum (averaged values over the basin). As in Fig. 5, spatial boxplots of ensemble dispersion in DHW annual maxima within each region are represented in Fig. 10c. Across regions, the spatial averages of dispersion (green markers and values in Fig. 10c) range between 0.25 and 0.49°C.weeks⁻¹, reached in





the NPSW and PEQD, respectively. Such uncertainties, with outliers reaching more than 1°C.weeks⁻¹ in all regions except NPSW, appear critical when comparing DHW values to the bleaching level of alert of 4°C.weeks⁻¹ defined by the NOAA (level 1 alert). This is further illustrated in Fig. 10b,d which show the number of level 1 alerts (ensemble mean) in the tropical Pacific, and the associated percentage of common alerts between all six products. The spatial average over the basin of the number of level 1 alerts for each product (not shown) revealed that OISST detected the most alerts closely followed by C3S, while the COMPOSITE detected the fewest, closely followed by CRW and GLORYS12v1. These results are in line with the maps of anomalies of Figure 9g-l and the previous observations. In most of the basin, the proportion of level 1 common alerts i.e. the common days for which DHW>=4°C.weeks⁻¹ across products ranges between less than 50% and 80% (Fig. 10d). In large areas of the basin (in ARC, in PEQD close to the south American coast and in PNEC), percentages of common alerts between all six products reach 70% at maximum. They even drop lower than 50% south of New Caledonia and in the Coral Sea (ARC). This means that among all bleaching alert days in these areas (which range between 1 and 2 weeks per year over 1993-2021 for ARC, Fig. 10b), at least one third or even a half was not detected by at least one of the six products evaluated here. These results confirm that SST product choice is also crucial to the DHW index.

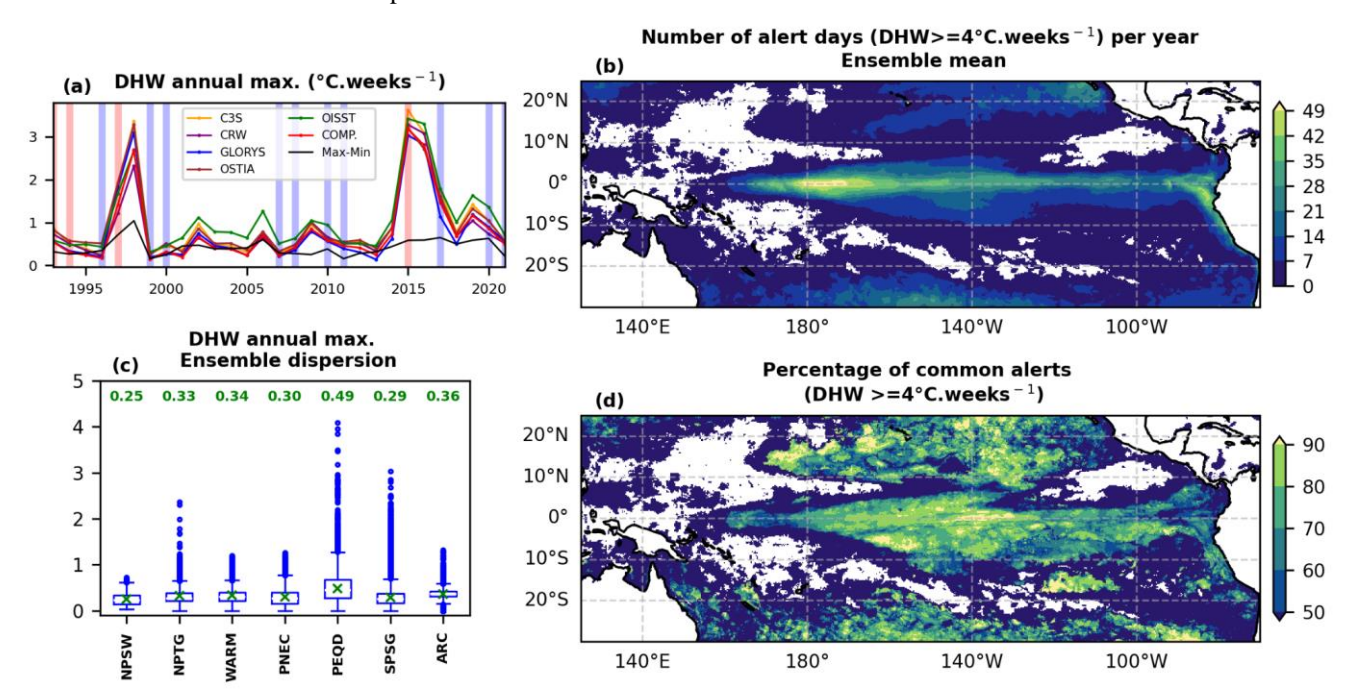


Figure 10: DHW analysis. (a) Yearly time-series of DHW annual maxima averaged over the tropical Pacific for each product. The black line represents the largest inter-product difference value for each year (maximum-minimum). The red and blue backgrounds indicate years of strong El Niño and La Niña, respectively, according to the Meiv2 index. (b) Ensemble mean of the number of level 1 alert days (DHW>=4°C.weeks⁻¹) per year, for each pixel of the tropical Pacific over 1993-2021. (c) Spatial boxplot of ensemble dispersion on DHW annual maxima within the study regions. The green marker represents the mean value, for which the exact value is indicated on top of the associated boxplot. (d) Percentage of common alerts of level 1 among the six SST products.



443

444

445

446

447

448

449

450

451

452

453

454

455

456

457

458

459

460

461

462

463

464 465

466

467

468

469

470

471

472

473

474



4- Discussion and conclusions

In this study, we have quantified the sensitivity of MHW metrics and DHW index to the SST product chosen in the tropical Pacific over 1993-2021, at both basin and regional scales. Uncertainties associated with the choice of the SST product were assessed using ensemble dispersion for each metric and region.

MHW mean metrics and temporal means of DHW annual maxima show similar spatial patterns in the tropical Pacific across

the six SST products evaluated. The observed spatial patterns of MHW metrics are consistent with previous regional (Holbrook

et al., 2022; Lal et al., 2025; Pagli et al., 2025) and global MHW studies (Oliver et al., 2021). However, products show

4.1- Inter-product differences and uncertainties

significant differences in the absolute values of the mean metrics and DHW index, which can go up to a factor of two (between OISST and GLORYS12v1). Over the basin, OISST detects the largest maximum intensity, onset rate, number of events and number of bleaching alerts, but the lowest duration, cumulative intensity and number of MHW days per year. On the opposite, the reanalysis GLORYS12v1 shows the largest number of MHW days per year, duration and cumulative intensity along with the lowest onset rate and second lowest maximum intensity, number of events and number of bleaching alerts. Such behaviors for MHW metrics were also observed by Lal et al. (2025) in the South Pacific island countries and by Wang et al. (2024) in the Northwest Pacific. The observed differences between these two products can be notably related to their strong and weak high-frequency SST variability (periods shorter than 2 weeks) respectively (cf. following section). Inter-product differences can lead to very different interpretations of the same extreme temperature event. As an example, SST time-series from the six products at one location off the eastern Australian Coast (147°E, 13°S) are shown for 2016, when a massive MHW occurred across the Southwest Pacific (Dutheil et al., 2024) causing important damage at the Great Barrier Reef (Great Barrier Reef Marine Park Authority report, 2017). The different time series reveal that this MHW was detected by all products (temperatures are above the 90th percentile from approximately February 2016 to September 2016, Fig. 11), but in very different ways (Fig. 11). The number of MHW events detected over the time period ranges from 3 (GLORYS12v1) to 9 (OSTIA), and the cumulative intensity of the MHWs detected from 78.9°C.days (OSTIA) to 182.1°C.days (GLORYS12v1). Consequently, interpretations linked to the biological impacts of such events, (e.g., which metrics have the greatest impact on ecosystems: the number of events? duration? recovery time?) can drastically vary from one SST product to another. Same issue applies to the DHW: for the example of Fig. 11, the level 1 alert for coral bleaching was not reached for C3S (3.34 °C.weeks⁻¹), and maximum DHW barely reached the alert threshold for GLORYS12v1 (4.09°C.weeks⁻¹) while it largely exceeded it for CRW (5.57°C.weeks⁻¹). More broadly, the percentage of level 1 bleaching alerts in common among the six products reaches at maximum ~60-70% in large areas of the tropical Pacific, especially in the ARC and PEQD close to coastal areas, where MHW biological impacts are crucial (Smith et al., 2024). Neo et al. (2023) also showed inconsistency in coral bleaching risk indicators between temperature data sources (among four evaluated) in northwestern and southeastern Australia. Let's note that DHW values computed here are lower than the ones of the NOAA CRW daily global 5km satellite



coral bleaching DHW product, probably due to differences in the MMM climatological baseline (1993-2021 in our study while years 1985-1990 plus 1993 only are used for CRW DHW product, Heron et al., 2014).

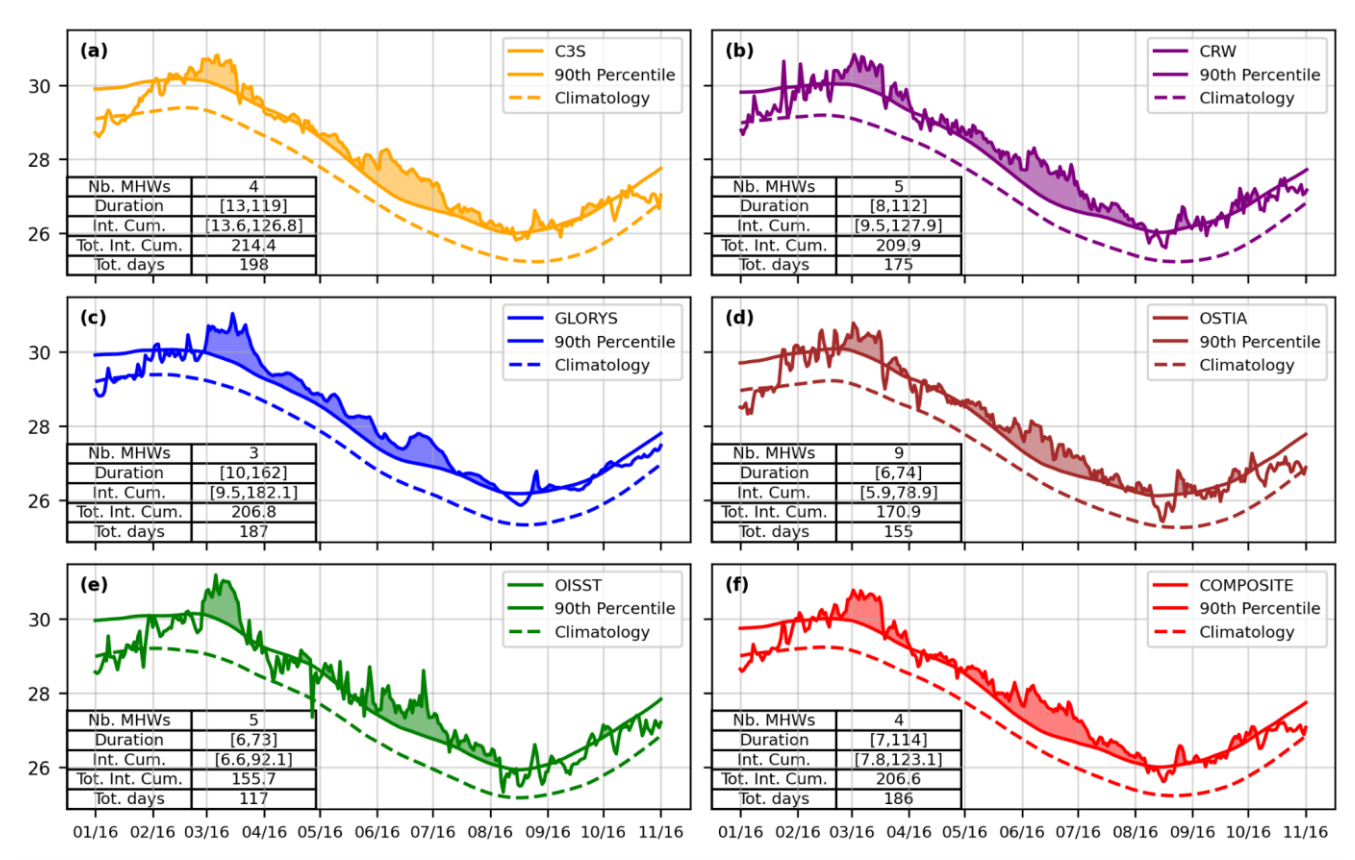


Figure 11: SST time-series of the six products at the same pixel (147E, 13S; off the eastern Australian coast) during the MHW event of 2016. The main MHW characteristics identified over the event period (January 2016 - November 2016) are indicated in the tables at the bottom left of each panel. Values in brackets represent the minimum and maximum duration and cumulative intensity of the detected events.

Regarding metrics sensitivity to the SST product choice, the onset rate is the most affected metric with the highest ensemble dispersion (between 24.2% in the ARC and 33.2% in the WARM) and lowest spatial correlation across all regions of the tropical Pacific. This metric should therefore be considered very carefully in MHW studies, especially since the onset rate determines the reaction window to a MHW, a key index for marine decision makers (Spillman et al., 2021). In contrast, the maximum intensity shows low ensemble dispersion (between 5.6% in the NPTG and 10.4% in the WARM) and high ensemble spatial correlation values in all regions, with a low interannual variability of both parameters in all regions, making it a robust metric regarding inter-product SST variability. Metrics with intermediate sensitivity - duration, cumulative intensity, number of events per year and number of MHW days per year - should be considered carefully as their ensemble dispersion, spatial correlation and interannual variability show high spatial differences. Consequently, SST product choice, region and study year might all influence these metrics.





Our results regarding MHW metrics differ from those of Marin et al. (2021). In their coastal MHW analysis, mean intensity strongly correlated with maximum intensity - showed the largest inter-product differences among the four datasets considered. This discrepancy may arise from several factors. First, methodological differences: Marin et al. (2021) assessed each product's deviation from the ensemble mean metric using a threshold based on ensemble dispersion to identify outliers and hotspot regions of inter-product differences (pixels with at least one outlier product). Such results depend on the individual product and ensemble mean MHW metrics, whereas our study gives an absolute value of the metric uncertainty by solely focusing on the ensemble dispersion. Second, we studied different types of events in different areas: Marin et al. (2021) focused on coastal MHWs worldwide on detrended SST time series while we studied all MHWs in the tropical Pacific without detrending. Third, the SST datasets differ: our ensemble includes both reanalysis and multi-product SST which show higher number of events and durations, whereas Marin et al. (2021) used only satellite-derived analyses.

Despite differences in metric robustness, our sensitivity analysis revealed that ensemble dispersion decreased and spatial correlation increased over time for all metrics and regions, reflecting the growing coherence between satellite SST datasets (Yang et al., 2021) and hence improvements in reanalysis products such as GLORYS12v1 (which assimilates satellite SST data) over the last decades. The intercomparison study of eight global gap-free SST products by Yang et al. (2021) indeed highlighted that global mean SST time series showed larger differences among products during the early period of the satellite era (1982-2002) when there were fewer observations.

To estimate an uncertainty in MHW metrics and DHW index, our sensitivity analysis also confirms the need for a regional approach, since ensemble dispersion values and their interannual variability vary across regions and metrics. A summary of uncertainties in each region for the six studied MHW metrics is provided in Fig. 5 and in Fig. 10 for the annual maximum of DHW. Within this regional framework, the WARM region particularly stands out across all MHW metrics, with dispersion values among products higher than 10% of the regional ensemble mean, making SST product choice particularly critical in this area for MHW analysis. Regarding DHW, the PEQD particularly stands out with uncertainty reaching 0.5°C.weeks⁻¹, which appears crucial when comparing to the level 1 of alert for coral bleaching.

Overall, the present inter-product comparison provides scientists uncertainty estimates and informs them about SST product limitations regarding the scope of their research.

4.2- Potential explanations of these differences

The use of different data sources (satellites with infrared or microwave sensors, geo-stationary or not, use of in-situ data or not, and if yes of various types - ships, drifting buoys, moored buoys, Argo), depths of SST estimations (skin layer, foundation), time of SST estimations (dusk to dawn, night-time only, daily mean) and the different data interpolation methods or assimilation methods in the SST products certainly explain the observed inter-product differences (Martin et al., 2012; Dash et al., 2012; Okuro et al. 2014; Fiedler et al., 2019; Huang et al., 2023). The MHW detection and DHW computation methods, both relying on thresholds, then amplifies small differences when computing MHW metrics and DHW.



525

526

527

528

529

530

531

532

533

534

535

536

537

538

539

540

541

542

543

544

545

546

547

548

549

550

551

552

553

554

555

556

557

558



Our results suggest that MHW detection is particularly sensitive to the high frequency variability of the SST signal. The combined analysis of the standard deviation of the high frequency SST signal (filtered at 15 days) in Appendix A (Fig. A1) and the radar chart of Fig. 3 suggest that spiky signals with stronger high frequency variability like OISST and OSTIA detect higher maximum intensity, onset rate and number of events, but lower duration, cumulative intensity and number of MHW days per year. On the opposite, smoother products like GLORYS12v1 or the COMPOSITE with lower high frequency variability (Fig. A1) detect lower maximum intensity, onset rate and number of events, but higher duration, cumulative intensity and number of MHW days per year (Fig. 3). Thus, the similarity of behaviours between GLORYS12v1 and the COMPOSITE (Fig. 3) might reflect the smoothing effect induced by the multi-product mean SST. These effects of high frequency variabilities were also seen in the SST time series of Fig. 11: climatological levels were similar between products, but OISST and OSTIA signals showed larger high frequency variability (confirmed by Fig. A1), which resulted in the detection of more MHWs of shorter durations (that duration reached 73 and 74 day maximum, respectively, Fig. 11), while GLORYS12v1 or the COMPOSITE showed smoother signals and detected fewer MHWs but of longer durations (duration of maximum 162 days for GLORYS12v1, Fig. 11). The spatial variability of common MHW days is also linked to the spatial scales of MHWs: low (high) percentages of common days correspond to areas with a high proportion of micro (macro) scale events. Indeed, the detection of macro scale MHWs (> $5^{\circ}x5^{\circ}$) was shown to be more robust across products compared to micro scale MHWs ($\leq 5^{\circ}x5^{\circ}$), with percentages of common MHW days for macro events largely higher than for micro events. The high proportions of micro MHWs (Fig. 7b) are also located in the areas of larger high frequency variability (Fig. A1): in the coastal areas of the PNEC, NPTG, ARC, in northern NPSW and along the Equator in the PEQD. Also, the duration, cumulative intensity, maximum intensity and onset rate show slightly higher dispersion values for micro-scale events than for macro-scale ones, but large differences are observed for the total MHW days and number of events per year, for which dispersion is higher by a factor of 2 for micro-scale events. Lal et al. (2025) similarly reported strong discrepancies in the number of micro-scale events across products whereas macro-scale events counts were relatively consistent. Consequently, a better understanding of the sensitivity of MHW detection for these spatially small events, as well as an improvement of SST products at these fine scales, might help to reduce the observed interproduct differences. The spatial correspondence between common MHW days across products and climatological precipitation patterns (i.e high precipitation; low percentages of common MHW days and vice versa) suggests that atmospheric conditions in convective areas of the SPCZ and the ITCZ (Brown et al., 2020) influence MHW detection. This effect may be linked to differences in signal retrieval and the handling of outliers in the presence of clouds and convective rainfall (for instance, there are spurious peaks in OISST induced by clouds, Reynolds et al., 2007). Alternatively, the particularly higher dispersion and lower ensemble spatial correlation values in the WARM region could also be explained by the specific MHW characteristics (short, numerous and spatially confined events that are difficult to detect). Nonetheless, the WARM region also shows the strongest decreasing rate in ensemble dispersion over time, suggesting that the growing coherence among satellite SST products in recent years (Yang et al., 2021) might have improved the detection of these short, small spatial scale and weak amplitude events.





4.3- Recommendations

Firstly, our results highlight the importance for MHW scientists to understand the behaviour of the SST product selected in their study, particularly its relative "ranking" compared to other products, which varies according to both the metric and the region considered (section 3.2) but also according to the time period of interest (as magnitude of inter-product differences varies between years, section 3.3.3). The evaluation of the high frequency variability of the SST signal can also give valuable information on the product chosen since it strongly influences MHW detection, as explained in section 4.2. Using several products for robustness is thus essential: because all SST products differ in their construction, we cannot a priori argue for a "best" dataset to be used for MHW detection without thorough evaluation against in situ and independent SST dataset. Yet, Fiedler et al., (2019) performed a comparison of SST datasets to in situ data and summed up the key strengths and weaknesses of various analyses compared to the others. Beyond characterizing product behaviour, MHW studies should also account for the uncertainty associated with SST product choice when reporting MHW metric estimates. When feasible, the use of several SST datasets can substantially increase the robustness of the results, by defining upper and lower bounds of metric estimates. The same recommendations apply for DHW studies, with other studies underlining the need to compare indicators of thermal stress from different data sets (Neo et al., 2023; Margaritis et al. 2025).

It is also worth noting that the sensitivity of MHW metrics to SST high-frequency variability may partly arise from the event

It is also worth noting that the sensitivity of MHW metrics to SST high-frequency variability may partly arise from the event definition itself: changing the minimum duration threshold (≥ 5 days) or the maximum gap to consider a continuous event (2 days) might affect the inter-product differences. More continuous indices, such as severity (Hobday et al., 2018; Sen Gupta et al., 2020) might help to reduce inter-product differences in MHW diagnostics.

Our results should also be interpreted carefully at finer scales, such as in coastal areas. Larger differences between satellite SST and in-situ temperature data were observed in coastal regions (Castro et al., 2012; Woo et al., 2020) compared to the overall accuracy of the SST in the global ocean and offshore regions. Woo et al. (2020) identified relationships between errors and coastal zones of vigorous tidal mixing, shallow bathymetry, and absence of microwave measurements. Significant differences between satellite and in-situ data were also observed in atolls and lagoons (Van Wynsberge et al., 2017).

Finally, regarding the relevance of a multi-product approach, our results highlight that the COMPOSITE does not show an intermediate "ranking" but rather follows the behaviour of the reanalysis product. Metric estimates from the COMPOSITE were influenced by the smoothing applied when averaging temperature data, which introduced biases in MHW statistics.

4.4- Perspectives

Our study focuses on the sensitivity of MHW metrics to the choice of the SST product. Yet, other methodological options not investigated in this study can also strongly impact the MHW estimates. Since trends in SST products show differences (Menemenlis et al., 2025), detrending SST time series might influence our results and should be investigated further. Also, as Smith et al. (2025) highlighted the significant influence of the baseline on MHW results, this choice might also impact our conclusions. Choosing other thresholds for MHW detection to focus on the most extreme events (e.g 98th percentile) might





also affect the observed inter-product differences. Similar remarks apply to the DHW, for which changing the accumulation window size or anomaly cutoff might impact our results. In addition, the re-gridding of SST datasets onto a common 0.25° grid might also have influenced our results. Indeed, computing spatial means for re-gridding tends to smooth SST time series, and might impact MHW detection and DHW computation. Since re-gridding is a common practice in MHW studies, more investigation on how much information is lost in the re-gridding process could help to advance MHW research. In the case of SST products intercomparison, Huang et al. (2023) showed that the intercomparison is influenced by whether SST products are in their original grids or preprocessed into common coarse grids.

As in Fiedler et al. (2019) with SST datasets, the comparison of our results to MHW metrics and DHW computed from in-situ and independent data could add valuable information to the study. Such comparison could help understand how the differences between SST products and in-situ SST data are translated through the MHW detection algorithm. However, in-situ data long enough to allow computation of MHWs are very sparse, and the depths of the estimated SST might differ, adding other biases in MHW metrics comparison. Extending our analysis at global scale could also give additional valuable information to users. For DHW computation, the comparison of our results to existing bleaching observations in some focus areas (as done by Neo et al. 2023 in northwestern and southwestern Australian reefs and Margaritis et al. 2025 in the Caribbean) could help to better understand the differences and similarities in bleaching risk indicators across datasets.

Including other re-analysis products in addition to GLORYS12v1 in our comparison could also be of interest to better understand the impact of the model and data-assimilation system considered in the different re-analyses on MHW detection, including on their vertical extent. This could be done in the framework of the MER-EP (Marine Environment Reanalysis Evaluation Project), a UN-Decade action led by Mercator-Ocean-International. The comparison of MHW metrics between multiple re-analyses could also benefit from the Observing System Experiments done in the framework of the Synergistic Observing Network for Ocean Prediction (SynObs) project (Fuji et al., 2024), if daily outputs are provided. Such comparisons could also help to quantify the influence of ocean observation systems on MHW metrics estimates.

In conclusion, this study reveals significant dispersion in key MHW metrics and provides new information on how the choice of the SST product impacts MHW detection and bleaching indices. This sensitivity should be kept in mind in future research on MHWs and the ecological impact of extreme temperature events, and the use of multiple SST products in such studies should be advocated to increase the robustness of the findings.

Authors contribution

CC, RLG, CM and SC designed the study and wrote the initial manuscript draft. CC performed the analysis presented in this manuscript. Discussions and iterative feedback from all co-authors significantly contributed to the revision of the manuscript.

this study were written in Python and can be shared upon request.



646



625 Competing interests 626 The authors declare that they have no conflict of interest. 627 628 Acknowledgments 629 We gratefully acknowledge Shilpa Lal for her help and relevant discussions which improved the paper, and Sébastien Petton 630 for his help to parallelize MHW detection code. We also thank colleagues from Mercator-Ocean-International for their advice. 631 The authors also acknowledge the Pôle de Calcul et de Données Marines (PCDM) for providing DATARMOR storage and 632 computational resources (http://www.ifremer.fr/). C.C is supported by the Institut français de recherche pour l'exploitation de 633 la mer (IFREMER) through a VSC funding (Volontariat Service Civique) at the Ifremer station of Vairao, Tahiti. The authors 634 acknowledge the support of the French National Research Agency under France 2030 (ANR-23-POCE-0001), as part of the 635 MaHeWa project (grant ANR-23-POCE-0001). This work was also supported by the French national program LEFE (les 636 enveloppes Fluides et l'environnement), project MaheWa-OO. 637 638 Data Availability Statement 639 All datasets used in this study are open source and available online. Temperature data from C3S, OSTIA and GLORYS12v1 640 available Copernicus are on 641 https://data.marine.copernicus.eu/product/SST GLO SST L4 REP OBSERVATIONS 010 024/description, 642 https://data.marine.copernicus.eu/product/SST GLO SST L4 REP OBSERVATIONS 010 011/description, 643 https://data.marine.copernicus.eu/product/GLOBAL MULTIYEAR PHY 001 030/description, respectively. The CRW data 644 were downloaded from https://coralreefwatch.noaa.gov/product/5km/index.php (via ftp). The OISSTv2 data were downloaded 645 from XXX https://psl.noaa.gov/data/gridded/data.noaa.oisst.v2.highres.html. All scripts used to obtain the results presented in





APPENDIX A

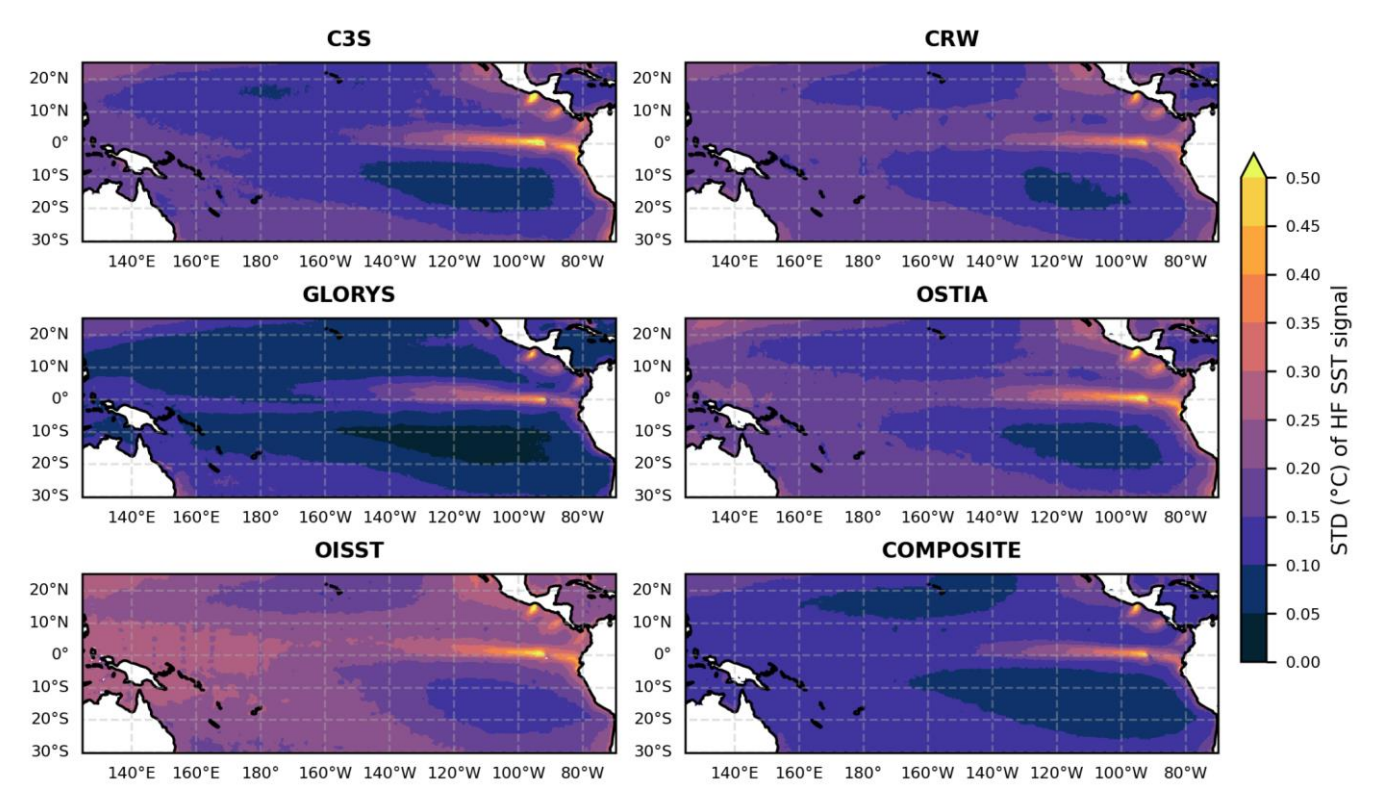


Figure A1. Standard deviation of the high frequency SST signal (high-pass filtered, half-power period of 15 days) over the period 1993-2021 for the six evaluated products.

References

- Amaya, D. J., Jacox, M. G., Fewings, M. R., Saba, V. S., Stuecker, M. F., Rykaczewski, R. R., Ross, A. C., Stock, C. A., Capotondi, A., Petrik, C. M., Bograd, S. J., Alexander, M. A., Cheng, W., Hermann, A. J., Kearney, K. A., and Powell, B. S.: Marine heatwaves need clear definitions so coastal communities can adapt, Nature, 616, 29–32, doi:10.1038/d41586-023-00924-2, 2023.
- Andréfouët, S., Dutheil, C., Menkes, C. E., Bador, M., and Lengaigne, M.: Mass mortality events in atoll lagoons: environmental control and increased future vulnerability, Glob. Change Biol., 21, 195–205, doi:10.1111/gcb.12699, 2015.
- Bian, C., Jing, Z., Wang, H., Wu, L., Chen, Z., Gan, B., and Yang, H.: Oceanic mesoscale eddies as crucial drivers of global marine heatwayes, Nat. Commun., 14, 2970, doi:10.1038/s41467-023-38811-z, 2023.





- Bonino, G., Masina, S., Galimberti, G., and Moretti, M.: Southern Europe and western Asian marine heatwaves (SEWA-
- 664 MHWs): A dataset based on macroevents, Earth Syst. Sci. Data, 15, 1269–1285. doi:10.5194/essd-15-1269-2023, 2023.

- Brown, J.R., Lengaigne, M., Lintner, B.R., Widlansky, M.J., van der Wiel, K., Dutheil, C., Linsley, B.B., Matthews, A.J. and
- 667 Renwick, J.: South Pacific Convergence Zone dynamics, variability and impacts in a changing climate, Nat. Rev. Earth
- 668 Environ., 1, 530–543, doi:10.1038/s43017-020-0078-2, 2020.

669

- 670 Capotondi A., Newman, M., , Xu T., and Di Lorenzo E.: An Optimal precursor of northeast Pacific marine heatwaves and
- 671 Central Pacific El Niño events, Geophys. Res. Lett. 49, e2021GL097350, doi:10.1029/2021GL097350, 2022.

672

- 673 Capotondi, A., Rodrigues, R. R., Sen Gupta, A., Benthuysen, J. A., Deser, C., Frölicher, T. L., Lovenduski, N. S., Amaya, D.
- J., Le Grix, N., Xu, T., Hermes, J., Holbrook, N. J., Martinez-Villalobos, C., Masina, S., Roxy, M. K., Schaeffer, A., Schlegel,
- R. W., Smith, K. E., and Wang, C.: A global overview of marine heatwaves in a changing climate, Commun. Earth Environ.,
- 5, 701, doi:10.1038/s43247-024-01806-9, 2024.

677

- 678 Chapman, C.C., Sloyan, B.M., Moore II, Thomas S., Reilly, J. A. and Matear, R.J.: Marine heatwaves in the East Australian
- 679 current modulated by mesoscale eddies, J. Geophys. Res. Oceans, 130, e2024JC021395, doi:10.1029/2024JC021395, 2025.
- Dash, P., Ignatov, A., Martin, M., Donlon, C., Brasnett, B., Reynolds, R.W., Banzon, V., Beggs, H., Cayula, J.-F., Chao, Y.,
- 681 Grumbine, R., Maturi, E., Harris, A., Mittaz, J., Sapper, J., Chin, T.M., Vazquez-Cuervo, J., Armstrong, E.M., Gentemann, C.,
- 682 Cummings, J., Piollé, J.-F., Autret, E., Roberts-Jones, J., Ishizaki, S., Høyer, J.L., and Poulter, D.: Group for High Resolution
- 683 Sea Surface Temperature (GHRSST) analysis fields inter-comparisons—Part 2: Near real time web-based level 4 SST Quality
- 684 Monitor (L4-SQUAM), Deep Sea Res. Part II: Top. Stud. Oceanogr., 77–80, 31-43, doi:10.1016/j.dsr2.2012.04.002, 2012.

685

- 686 Castro, S. L., Wick, G.A., and Emery, W.J.: Evaluation of the relative performance of sea surface temperature measurements
- from different types of drifting and moored buoys using satellite-derived reference products, J. Geophys. Res., 117, C02029,
- 688 doi:10.1029/2011JC007472, 2012.

689

- Dee, D. P., Uppala, S. M., Simmons, A. J., Berrisford, P., Poli, P., Kobayashi, S., Andrae, U., Balmaseda, M. A., Balsamo, G.,
- 691 Bauer, P., Bechtold, P., Beljaars, A. C. M., Van De Berg, L., Bidlot, J., Bormann, N., Delsol, C., Dragani, R., Fuentes, M.,
- 692 Geer, A. J., Haimberger, L., Healy, S. B., Hersbach, H., Hólm, E. V., Isaksen, L., Kållberg, P., Köhler, M., Matricardi, M.,
- 693 McNally, A. P., Monge-Sanz, B. M., Morcrette, J. -J., Park, B. -K., Peubey, C., De Rosnay, P., Tavolato, C., Thépaut, J. -N.,
- and Vitart, F.: The ERA-Interim reanalysis: configuration and performance of the data assimilation system, Q. J. R. Meteorol.
- 695 Soc., 137, 553–597, doi:10.1002/qj.828, 2011.





- Donlon, C.J., Martin M., Stark J., Roberts-Jones J., Fiedler E., and Wimmer W.: The Operational Sea Surface Temperature
- and Sea Ice Analysis (OSTIA) system, Remote Sens. Environ., 116, 140–158, doi:10.1016/j.rse.2010.10.017, 2012.

- Dutheil, C., Lal, S., Lengaigne, M., Cravatte, S., Menkès, C., Receveur, A., Börgel, F., Gröger, M., Houlbreque, F., Le Gendre,
- 701 R., Mangolte, I., Peltier, A., and Meier, H. E. M.: The massive 2016 marine heatwave in the Southwest Pacific: An "El Niño-
- Madden-Julian Oscillation" compound event, Sci. Adv., 10, eadp2948, doi:10.1126/sciadv.adp2948, 2024.

703

- Farchadi, N., McDonnell, L.H., Ryan, S., Lewison, R.L. and Braun, C.D.: Marine heatwaves are in the eye of the beholder,
- 705 Nat. Clim. Chang. 15, 236–239, doi:10.1038/s41558-025-02257-6, 2025.

706

- Fiedler, K.E., McLaren, A., Banzon, V., Brasnett, B., Ishizaki, S., Kennedy, J., Rayner, N., Roberts-Jones, J., Corlett, G.,
- 708 Merchant, C.J and Donlon, C.: Intercomparison of long-term sea surface temperature analyses using the GHRSST Multi-
 - Product Ensemble (GMPE) system, Remote Sens., 222, 18-33, doi:10.1016/j.rse.2018.12.015, 2019.

709710

- 711 Frölicher, T.L., Fischer, E.M. and Gruber, N.: Marine heatwayes under global warming, Nature, 560, 360-364,
- 712 doi:10.1038/s41586-018-0383-9, 2018.

713

- 714 Fujii, Y., Remy, E., Balmaseda, M.A., Kido, S., Waters, J., Peterson, K.A., Smith, G.C., Ishikawa, I. and Chikhar, K.: The
- 715 international multi-system OSEs/OSSEs by the UN Ocean Decade Project SynObs and its early results, Front. Mar. Sci., 11,
- 716 1476131, doi:10.3389/fmars.2024.1476131, 2024.

717

- 718 Great Barrier Reef Marine Park Authority 2017, Final report: 2016 coral bleaching event on the Great Barrier Reef, GBRMPA,
- 719 Townsville.

720

- Hartog, J. R., Spillman, C. M., Smith, G. and Hobday, A. J. Forecasts of marine heatwaves for marine industries: reducing
- 722 risk, building resilience and enhancing management responses, Deep Sea Res. Part II Top. Stud. Oceanogr., 209, 105276,
- 723 doi:10.1016/j.dsr2.2023.105276, 2023.

724

- Heron, S.F., Liu, G., Eakin, C.M., Skirving, W.J., Muller-Karger, F.E., Vega-Rodriguez, M., De La Cour, J.L., Burgess, T.F.
- and Strong, A.E.: Climatology development for NOAA Coral Reef Watch's 5-km product suite, NOAA technical report
- 727 NESDIS, 145, doi:10.7289/V59C6VBS, 2014.

- Hersbach, H., Bell, B., Berrisford, P., Hirahara, S., Horányi, A., Muñoz-Sabater, J., Nicolas, J., Peubey, C., Radu, R., Schepers,
- D., Simmons, A., Soci, C., Abdalla, S., Abellan, X., Balsamo, G., Bechtold, P., Biavati, G., Bidlot, J., Bonavita, M., De Chiara,



735

739

743

747

751

754

758



- G., Dahlgren, P., Dee, D., Diamantakis, M., Dragani, R., Flemming, J., Forbes, R., Fuentes, M., Geer, A., Haimberger, L.,
- Healy, S., Hogan, R. J., Hólm, E., Janisková, M., Keeley, S., Laloyaux, P., Lopez, P., Lupu, C., Radnoti, G., de Rosnay, P.,
- Rozum, I., Vamborg, F., Villaume, S., and Thépaut, J.-N.: The ERA5 global reanalysis, Q. J. R. Meteorol. Soc., 146, 1999–
- 734 2049, doi:10.1002/qj.3803, 2020.
- Hobday, A. J., Alexander, L. V., Perkins, S. E., Smale, D. A., Straub, S. C., Oliver, E. C. J., Benthuysen, J. A., Burrows, M.
- T., Donat, M. G., Feng, M., Holbrook, N. J., Moore, P. J., Scannell, H. A., Sen Gupta, A., and Wernberg, T.: A hierarchical
- 738 approach to defining marine heatwayes, Prog. Oceanogr., 141, 227–238, doi:10.1016/j.pocean.2015.12.014, 2016.
- Hobday, A. J., Oliver, E. C. J., Gupta, A. S., Benthuysen, J. A., Burrows, M. T., Donat, M. G., Holbrook, N. J., Moore, P. J.,
- 741 Thomsen, M. S., Wernberg, T., and Smale, D. A.: Categorizing and Naming MARINE HEATWAVES, Oceanography, 31,
- 742 162–173, doi:10.5670/oceanog.2018.205, 2018.
- Hobday, A.J., Burrows, M.T., Filbee-Dexter, K., Holbrook, N.J., Sen Gupta, A., Smale, D.A., Smith, K.E., Thomsen, M.S.
- and Wernberg, T.: With the arrival of El Nino, prepare for stronger marine heatwaves, Nature, 621, 38–41,
- 746 doi:10.1038/d41586-023-02730-2, 2023.
- Holbrook, N. J., Scannell, H. A., Sen Gupta, A., Benthuysen, J. A., Feng, M., Oliver, E. C. J., Alexander, L. V., Burrows, M.
- 749 T., Donat, M. G., Hobday, A. J., Moore, P. J., Perkins-Kirkpatrick, S. E., Smale, D. A., Straub, S. C., and Wernberg, T.: A
- global assessment of marine heatwaves and their drivers, Nat. Commun., 10, 2624, doi:10.1038/s41467-019-10206-z, 2019.
- 752 Holbrook, N.J., Sen Gupta, A., Oliver, E.C.J., Hobday, A.J., Benthuyssen, J.A, Scannell, H.A., Smale, D.A. and Wernberg,
- 753 T.: Keeping pace with marine heatwayes, Nat. Rev. Earth Environ., 1, 482–493, doi:10.1038/s43017-020-0068-4, 2020.
- Holbrook, N. J., Hernaman, V., Koshiba, S., Lako, J., Kajtar, J. B., Amosa, P., and Singh, A.: Impacts of marine heatwaves on
- 756 tropical western and central Pacific Island nations and their communities, Glob. Planet. Change, 208, 103680,
- 757 doi:10.1016/j.gloplacha.2021.103680, 2022.
- Huang, B., Liu, C., Banzon, V., Freeman, E., Graham, G., Hankins, B., Smith, T., and Zhang, H.-M.: Improvements of the
- 760 Daily Optimum Interpolation Sea Surface Temperature (DOISST) Version 2.1, J. Clim., 34, 2923–2939, doi:10.1175/JCLI-D-
- 761 20-0166.1, 2021.
- Huang, B., Yin, X., Carton, J. A., Chen, L., Graham, G., Liu, C., Smith, T., & Zhang, H.: Understanding Differences in Sea
- Surface Temperature Intercomparisons, J. Atmos. Oceanic Technol., 40(4), 455-473. doi:10.1175/JTECH-D-22-0081.1, 2023.



765

771

774

778

781

787

790



- 766 Intergovernmental Panel on Climate Change (IPCC), 2001: Appendix 12.3: Pattern Correlation Methods. In: Climate Change
- 767 2001: The Scientific Basis. Contribution of Working Group I to the Third Assessment Report of the Intergovernmental Panel
- on Climate Change [Houghton, J.T., Y. Ding, D.J. Griggs, M. Noguer, P.J. van der Linden, X. Dai, K. Maskell, and C.A.
- 769 Johnson (eds.)]. Cambridge University Press, Cambridge, United Kingdom and New York, NY, USA. Available at:
- https://archive.ipcc.ch/ipccreports/tar/wg1/470.htm
- Kajtar, J.B., Holbrook, N.J., Lyth, A., Hobday, A.J., Mundy, C.N. and Ugalde, S.C.: A stakeholder-guided marine heatwave
- hazard index for fisheries and aquaculture, Clim. Change, 177, 26, doi:10.1007/s10584-024-03684-8, 2024.
- Lal, S., Cravatte, S., Menkes, C., Macdonald, J., LeGendre, R., Mangolte, I., Dutheil, C., Holbrook, N., and Nicol, S.:
- 776 Characterization of Past Marine Heatwaves around South Pacific Island Countries: What really matters?, EGUsphere, 1, 48,
- 777 doi:10.5194/egusphere-2025-3281, 2025.
- Langlais, C., Lenton, A., Heron, S., Evenhuis, C., Sen Gupta, A., Brown, J.N. and Kuchinke, M.: Coral bleaching pathways
- under the control of regional temperature variability, Nature Clim. Change, 7, 839–844, doi:10.1038/nclimate3399, 2017.
- 782 Lellouche, J.-M., Greiner, E., Bourdallé-Badie, R., Garric, G., Melet, A., Drévillon, M., Bricaud, C., Hamon, M., Le Galloudec,
- O., Regnier, C., Candela, T., Testut, C.-E., Gasparin, F., Ruggiero, G., Benkiran, M., Drillet, Y., Le Traon, P.-Y., Bourdallé-
- Badie, R., Garric, G., Melet, A., Drévillon, M., Bricaud, C., Hamon, M., Le Galloudec, O., Regnier, C., Candela, T., Testut,
- 785 C.-E., Gasparin, F., Ruggiero, G., Benkiran, M., Drillet, Y., and Le Traon, P.-Y.: The Copernicus Global 1/12° Oceanic and
- 786 Sea Ice GLORYS12 Reanalysis, Front. Earth Sci., 9, 698876, doi:10.3389/feart.2021.698876, 2021.
- 788 Li, J., Roughan, M., and Hemming, M.: Interactions between cold cyclonic eddies and a western boundary current modulate
- 789 marine heatwayes, Commun. Earth & Environ., 4(1), 1–11. doi:10.1038/s43247-023-01041-8, 2023.
- Longhurst, A. R., Chapter 7 PROVINCES: THE SECONDARY COMPARTMENTS, in: Ecological Geography of the Sea,
- 792 2nd ed., edited by A. R. Longhurst, Academic Press, Burlington, 103–114, doi:10.1016/B978-012455521-1/50008-5, 2007.
- Madec, G., Bell, M., Benshila, R., Blaker, A., Boudrallé-Badie, R., Bricaud, C., Bruciaferri, D., Carneiro, D., Castrillo, M.,
- 795 Calvert, D., Chanut, J., Clementi, E., Coward, A., Lavergne, C. de, Dobricic, S., Epicoco, I., Éthé, C., Fiedler, E., Ford, D.,
- Furner, R., Ganderton, J., Graham, T., Harle, J., Hutchinson, K., Iovino, D., King, R., Lea, D., Levy, C., Lovato, T.,
- Maisonnave, E., Mak, J., Sanchez, J. M. C., Martin, M., Martin, N., Martins, D., Masson, S., Mathiot, P., Mele, F., Mocavero,
- S., Moulin, A., Müller, S., Nurser, G., Oddo, P., Paronuzzi, S., Paul, J., Peltier, M., Person, R., Rousset, C., Rynders, S.,





- 799 Samson, G., Schroeder, D., Storkey, D., Storto, A., Téchené, S., Vancoppenolle, M., and Wilson, C.: NEMO Ocean Engine
- 800 Reference Manual, doi:10.5281/zenodo.14515373, 2024.

- Madden, R. A., and Julian, P.R.: Detection of a 40–50 day oscillation in the zonal wind in the tropical Pacific, J. Atmos. Sci.,
- 803 28, 702–708, doi:10.1175/1520-0469, 1971.

804

- Madden, R. A., and Julian, P.R.: Description of global-scale circulation cells in the tropics with a 40–50 day period, J. Atmos.
- 806 Sci., 29, 1109–1123, doi:10.1175/1520-0469, 1972.

807

- 808 Margaritis, G., Kent, E.C. and Foster, G.L.: Intercomparison of satellite-derived SST with logger data in the Caribbean—
- 809 Implications for coral reef monitoring, PLOS Climate 4(1): e0000480, doi:10.1371/journal.pclm.0000480, 2025.

810

- Marin M., Feng, M., Phillips, H.E. and Bindoff, N.L.: A Global, Multiproduct Analysis of Coastal Marine Heatwaves:
- Distribution, Characteristics, and Long-Term Trends, JGR oceans, 126, 2, doi:10.1029/2020JC016708, 2021.

813

- Martin, M., Dash, P., Ignatov, A., Banzon, V., Beggs, H., Brasnett, B., Cayula, J.-F., Cummings, J., Donlon, C., Gentemann,
- 815 C., Grumbine, R., Ishizaki, S., Maturi, E., Reynolds, R. W. and Roberts-Jones, J.: Group for High Resolution Sea Surface
- Temperature (GHRSST) analysis fields inter-comparisons. Part 1: A GHRSST multi-product ensemble (GMPE), Deep Sea
- 817 Res. Part II: Top. Stud. Oceanogr., 77–80, 21–30, doi:10.1016/j.dsr2.2012.04.013, 2012.

818

- Menemenlis, S., Vecchi, G.A., Yang, W, Fueglistaler, S. and Raghuraman, S.P.: Consequential differences in satellite-era sea
- surface temperature trends across datasets, Nat. Clim. Chang., 15, 897–903, doi:10.1038/s41558-025-02362-6, 2025.

821

- Merchant, C.J., Allan, R.P. and Embury, O.: Quantifying the acceleration of multidecadal global sea surface warming driven
 - by Earth's energy imbalance, Environ. Res. Lett., 20, 024037, doi:10.1088/1748-9326/adaa8a, 2025.

823 824

- Misra, R., Sérazin, G., Meissner, K. J. and Gupta, A.S.: Projected changes to Australian marine heatwaves, Geophys. Res.
- 826 Lett., 48, e2020GL091323, doi:10.1029/2020GL091323, 2021.

827

- Neo, V. H. F., Zinke, J., Fung, T., Merchant, C. J., Zawada, K. J. A., Krawczyk, H., and Maina, J. M.: Inconsistent coral
- 829 bleaching risk indicators between temperature data sources, Earth and Space Science, 10, e2022EA002688.
- 830 doi:10.1029/2022EA002688, 2023.





- Okuro, A., Kubota, M., Tomita, H., and Hihara, T.: Inter-comparison of various global sea surface temperature products, Int.
- 833 J. Remote Sens., 35(14), 5394-5410, doi:10.1080/01431161.2014.926415, 2014.

- Oliver E.C.J., Burrows M.T., Donat M.G., Sen Gupta A., Alexander L.V., Perkins-Kirkpatrick S.E., Benthuysen J.A., Hobday
- 836 A.J., Holbrook N.J., Moore P.J., Thomsen M.S., Wernberg T. and Smale D.A.: Projected Marine Heatwaves in the 21st Century
- and the Potential for Ecological Impact, Front. Mar. Sci., 6, 734, doi:10.3389/fmars.2019.00734, 2019.

838

- Oliver, E. C. J., Benthuysen, J. A., Darmaraki, S., Donat, M. G., Hobday, A. J., Holbrook, N. J., Schlegel, R. W., and Gupta,
- A. S.: Marine Heatwayes, Annu. Rev. Mar. Sci., 13, 313–342, doi:10.1146/annurev-marine-032720-095144, 2021.

841

- Pagli, B., Izumo, T., Barboni, A., Chevillard, C., Dutheil, C., Legrand, R., Menkes, C., Rocuet, C., and Cravatte, S.: Marine
- Heatwaves across the central South Pacific: characteristics, mechanisms, and modulation by the El Niño Southern Oscillation,
- 844 EGUsphere [preprint], doi:10.5194/egusphere-2025-4166, 2025.

845

- Pearce, A., Lenanton, R., Jackson, G., Moore, J., Feng, M. and Gaughan, D.: The "marine heat wave" off Western Australia
- during the summer of 2010/11, Fisheries Research Report No. 222, Department of Fisheries, Western Australia. 40pp., 2011.

848

- Reynolds, R. W., Smith, T. M., Liu, C., Chelton, D.B., Casey, K.S. and Schlax, M.G.: Daily High-Resolution-Blended
- 850 Analyses for Sea Surface Temperature, J. Climate, 20, 5473–5496, doi:10.1175/2007JCLI1824.1, 2007.

851

852 Schulzweida, U., CDO User Guide (2.3.0), Zenodo, doi:10.5281/zenodo.10020800, 2023.

853

- 854 Sen Gupta, A., Thomsen, M., Benthuysen, J. A., Hobday, A. J., Oliver, E., Alexander, L. V., Burrows, M. T., Donat, M. G.,
- Feng, M., Holbrook, N. J., Perkins-Kirkpatrick, S., Moore, P. J., Rodrigues, R. R., Scannell, H. A., Taschetto, A. S.,
- 856 Ummenhofer, C. C., Wernberg, T., and Smale, D. A.: Drivers and impacts of the most extreme marine heatwave events, Sci.
- 857 Rep., 10, 19359, doi:10.1038/s41598-020-75445-3, 2020.

858

- 859 Skirving, W., Marsh, B., De La Cour, J., Liu, G., Harris, A., Maturi, E., Geiger, E., and Eakin, C. M.: CoralTemp and the Coral
- Reef Watch Coral Bleaching Heat Stress Product Suite Version 3.1, Remote Sens., 12, 3856, doi:10.3390/rs12233856, 2020.

861

- 862 Smith, K. E., Burrows, M. T., Hobday, A. J., Sen Gupta, A., Moore, P. J., Thomsen, M., Wernberg, T., and Smale, D. A.:
- 863 Socioeconomic impacts of marine heatwaves: Global issues and opportunities, Science, 374(6566), eabi3593,
- 864 doi:10.1126/science.abj3593, 2021.





- 866 Smith, K.E., Aubin, M., Burrows, M.T., Filbee-Dexter, K., Hobday, A.J., Holbrook, N.J., King, N.G., Moore, P.J., Sen Gupta,
- A., Thomsen, M., Wernberg, T., Wilson, E. and Smale, D.A.: Global impacts of marine heatwaves on coastal foundation
- 868 species, Nat. Commun., 15, 5052, doi:10.1038/s41467-024-49307-9, 2024.

- 870 Smith, K. E., Sen Gupta, A., Amaya, D., Benthuysen, J. A., Burrows, M. T., Capotondi, A., Filbee-Dexter, K., Frölicher, T.
- 871 L., Hobday, A. J., Holbrook, N. J., Malan, N., Moore, P. J., Oliver, E.C. J., Richaud, B., Salcedo-Castro, J., Smale, D. A.,
- Thomsen, M., and Wernberg, T.: Baseline matters: Challenges and implications of different marine heatwave baselines, Prog.
- 873 Oceanogr., 231, 103404, doi:10.1016/j.pocean.2024.103404, 2025.

874

- 875 Spillman C.M., Smith G.A., Hobday A.J. and Hartog J.R.: Onset and Decline Rates of Marine Heatwaves: Global Trends,
- Seasonal Forecasts and Marine Management, Front. Clim., 3, 801217, doi:10.3389/fclim.2021.801217, 2021.

877

- 878 Spillman C.M., Hobday, A.J., Behrens, E., Feng, M., Capotondi. A., Cravatte, S., Holbrook, N.J. and Sen Gupta, A.: What
- 879 makes a marine heatwave forecast useable, useful and used? Prog. Oceanogr., 234, 103464,
- 880 doi:10.1016/j.pocean.2025.103464, 2025.

881

- 882 Terhaar, J., Burger, F.A., Vogt, L., Frölicher, T.L. and Stocker, T.F.: Record sea surface temperature jump in 2023–2024
- unlikely but not unexpected, Nature, 639, 942–946, doi:10.1038/s41586-025-08674-z, 2025.

884

- Van Wynsberge, S., Menkes, C., Le Gendre, R., Passfield, T. and Andréfouët, S.: Are Sea Surface Temperature satellite
- measurements reliable proxies of lagoon temperature in the South Pacific?, Estuarine, Coastal and Shelf Science, 199, 117-
- 887 124, doi:10.1016/j.ecss.2017.09.033, 2017.

888

- Yang, C., Leonelli, F. E., Marullo, S., Artale, V., Beggs, H., Nardelli, B. B., Chin, T. M., De Toma, V., Good, S., Huang, B.,
- Merchant, C. J., Sakurai, T., Santoleri, R., Vazquez-Cuervo, J., Zhang, H., & Pisano, A.: Sea Surface Temperature
- 891 Intercomparison in the Framework of the Copernicus Climate Change Service (C3S), J. Climate, 34(13), 5257-5283.
- 892 doi:10.1175/JCLI-D-20-0793.1, 2021.

893

- Wang, H., Lu, Y., Zhai, L., Chen, X. and Liu, S.: Variations of surface marine heatwaves in the Northwest Pacific during
- 895 1993–2019, Front. Mar. Sci., 11, 1323702, doi:10.3389/fmars.2024.1323702, 2024.

- 897 Woo, H.-J., and Park, K.-A.: Inter-Comparisons of Daily Sea Surface Temperatures and In-Situ Temperatures in the Coastal
- 898 Regions. Remote Sens., 12(10), 1592, doi:10.3390/rs12101592, 2020.